Development and Evaluation of a Detailed Mechanism for the Atmospheric Reactions of Isoprene and NO_x

William P. L. Carter[*1] and Roger Atkinson[2]

International Journal of Chemical Kinetics
in press

January 12, 1996

[*]Author to whom correspondence should be addressed.

[1]Statewide Air Pollution Research Center and
College of Engineering, Center for Environmental Research and Technology
University of California, Riverside, CA 92521

[2]Statewide Air Pollution Research Center and
Department of Soil and Environmental Sciences
University of California, Riverside, CA 92521

MNS-96:CARTER.KIN

ABSTRACT

A detailed atmospheric photochemical mechanism for the atmospheric reactions of isoprene its major oxidation products in the presence of NO_x, which incorporates the most recent laboratory results and our current understanding of the system, is described. It is evaluated by comparing its predictions against results of NO_x-air irradiations of isoprene and its two major products, methacrolein, and methyl vinyl ketone (MVK), in five different types of environmental chambers at two different laboratories. In most cases it simulated experimental results within the uncertainty of the data and the chamber and run characterization model. However, the photodecomposition quantum yields of methacrolein and MVK and the organic nitrate yield from the OH + isoprene reaction had to be adjusted to obtain satisfactory simulations of the data. The major discrepancy observed was that the model tended to underpredict PAN by ~40% in the isoprene experiments, despite the fact that the model predicted PAN from methacrolein and MVK reasonably well. The uncertainties and additional data needed to completely characterize the isoprene atmospheric photooxidation system are discussed.

Keywords

Isoprene, Methacrolein, Methyl Vinyl Ketone, Biogenic Hydrocarbons, Photochemical Smog, Ozone, Air Quality, Airshed Models, Environmental Chambers.

INTRODUCTION

Isoprene is emitted in substantial quantities from certain types of vegetation [1-6], and is believed to play an important role in both urban and rural ozone formation [7-9]. It is therefore important that its atmospheric oxidation reactions be understood and correctly represented in computer airshed models used to simulate urban and regional air quality, and various representations of isoprene photooxidation chemistry are included in almost all urban or regional airshed models currently in use for research or regulatory purposes. Chemical mechanisms for isoprene photooxidation have been developed for use in computer models by Lloyd *et al*. [10], Gery *et al*. [11,12] (Carbon Bond CB-IV), Stockwell *et al*. [13] (RADM-2) and Carter [14] (SAPRC-90). The SAPRC-90 and RADM-2 mechanisms represent the carbonyl oxidation products of isoprene by acetaldehyde or propanal, while the CB-IV mechanism uses ethene and other species for this purpose. Therefore, these three

mechanisms use highly condensed, and now dated, representations of the atmospheric reactions of isoprene.

More recently, Paulson and Seinfeld [15] developed a detailed, explicit photooxidation mechanism for isoprene which reflected the knowledge of isoprene atmospheric chemistry circa 1992. However, a number of more recent studies have shown that the formation yields of OH radicals, $O(^3P)$ atoms, 1,2-epoxymethylbutenes, methacrolein and methyl vinyl ketone (MVK) from the O_3 reaction with isoprene employed by Paulson and Seinfeld [15] require significant revision [16-18]. Furthermore, a number of studies have recently measured the ambient atmospheric concentrations of isoprene, methacrolein, methyl vinyl ketone and 3-methylfuran and used the laboratory kinetic and product data to help elucidate the ambient air data [19-23].

The major reactions of isoprene in the atmosphere are with OH radicals, NO_3 radicals and O_3 [24], and the rate constants for these reactions are reliably known [24-26]. Additionally, reactions of isoprene with $O(^3P)$ atoms and NO_2 can be significant under high NO_x conditions or in environmental chamber experiments [27]. While the kinetics of these reactions now appear to be well known [24,28], there are significant areas of uncertainty in the products and mechanisms of these reactions of isoprene [24]. The current status of the OH radical, NO_3 radical, $O(^3P)$ atom and O_3 reactions is briefly discussed below.

The reaction of the OH radical with isoprene proceeds almost entirely by initial addition of the OH radical to the >C=C< bonds [25]. Formaldehyde, methacrolein, methyl vinyl ketone and 3-methylfuran have been identified and quantified as products of the OH radical reaction [27,29-31], but only account for only ~55-60% of the reacting carbon in the presence of NO [27,30,31] and even less in the absence of NO [31]. In the presence of NO, the remaining products are postulated to include organic nitrates [30] and hydroxycarbonyls [27,30], and Kwok *et al*. [32] have observed C_4- and C_5-hydroxycarbonyls from the OH radical reaction with isoprene in the presence of NO using atmospheric pressure ionization mass spectrometry (API-MS). In addition, using a pentafluorobenzyl-hydroxylamine hydrochloride derivitization method combined with gas chromatography and ion trap mass spectrometry, Yu *et al*. [33] observed and determined molecular weights for various unidentified C_4- and C_5-unsaturated hydroxycarbonyls, C_5-unsaturated carbonyls, glyoxal, methylglyoxal, hydroxyacetone and glycolaldehyde in isoprene - NO_x - air smog chamber experiments. (Many of these compounds are expected as secondary products.) However, at the present time the specific

identities and formation yields of the hydroxycarbonyls and nitrates are not known, nor are the subsequent atmospheric reactions of these products.

The reaction of isoprene with O_3 proceeds by initial addition of O_3 to the double bonds to form two primary ozonides, each of which then decomposes to two sets of (carbonyl plus biradical) [18,34] or, apparently, to a 1,2-epoxymethylbutene plus O_2 as a minor channel [17]. This mechanism is consistent with the observed formation of formaldehyde, methacrolein, methyl vinyl ketone, 1,2-epoxy-2-methyl-3-butene and 1,2-epoxy-3-methyl-3-butene from the O_3 reaction. However, apart from the observation that OH radicals are formed in significant yield from the O_3 reaction with isoprene [16,34] (with a yield of $0.27\ ^{+0.13}_{-0.09}$ [16]), little is known concerning the reactions of the biradical intermediates, or the products they ultimately form.

The products of the NO_3 radical reaction with isoprene are the least well understood [24]. The *in situ* Fourier transform infrared (FT-IR absorption spectroscopic study of Skov *et al*. [35] indicated that NO_3 radical addition at the 1-position dominated over addition at the 4-position, and that the nitratocarbonyl $O_2NOCH_2C(CH_3)=CHCHO$ was the major product, with other C_5-nitratocarbonyls and hydroxycarbonyls being formed as minor products. The API-MS study of Kwok *et al*. [36] shows that C_5-nitratocarbonyls, hydroxycarbonyls and nitratohydroperoxides are formed, together with C_5-hydroxycarbonyls (assumed to arise from the isomerization of nitrato-alkoxy radicals), and these data [36] are consistent with those of Skov *et al*. [35] and with the general reaction pathways discussed by Atkinson [24,26].

The major products identified and, in some cases, quantified from the isoprene reactions with OH radicals, NO_3 radicals and O_3 (for example, methacrolein, methyl vinyl ketone, and hydroxy- and nitrato-substituted unsaturated C_5-carbonyls) are expected to be reactive towards OH radicals and O_3, and their subsequent reactions are therefore expected to contribute significantly to the overall ozone-forming potential of isoprene. Although the kinetics and products of the OH radical reactions of methacrolein and methyl vinyl ketone appear to be relatively well understood [24,37,38], the products and mechanisms of their NO_3 radical and O_3 reactions are more uncertain than is the case for the corresponding reactions of isoprene. Furthermore, the possibility that methacrolein and methyl vinyl ketone photolyze at significant rates in the atmosphere has not been ruled out. The C_5-hydroxyaldehydes are expected to be even more reactive, yet there is no information at all concerning their mechanisms or even their primary rate constants.

Because of these uncertainties, no isoprene mechanism, no matter how detailed, can be relied upon to give accurate predictions of the effects of isoprene emissions on ozone formation, radical levels, and other measures of air quality unless it can be shown to adequately simulate these observations under controlled conditions in environmental chamber experiments. Because of the importance of isoprene in air quality models, the U.S. Environmental Protection Agency has over the years funded environmental chamber experiments which can be used for testing isoprene oxidation mechanisms. In the early 1980's, a number of isoprene - NO_x - air experiments were carried out in the University of North Carolina (UNC) outdoor chamber facility, and these were used to develop the largely parameterized isoprene mechanism used in the CB-IV mechanism [11,12]. In the mid-1980's, several isoprene - NO_x - air, methacrolein - NO_x - air and methyl vinyl ketone - NO_x - air irradiations were carried out in the indoor chambers at the Statewide Air Pollution Research Center (SAPRC) at the University of California at Riverside [39], and these experiments together with the UNC runs were used in the evaluations of the SAPRC-90 and RADM-2 mechanisms [40,41]. These evaluations showed that the SAPRC-90 and RADM-2 isoprene mechanisms did not perform well in simulating O_3 data in the UNC or SAPRC chamber experiments, suggesting that they would probably not give reliable predictions of the effects of isoprene emissions on O_3 in the atmosphere. The mechanism of Paulson and Seinfeld [15] was developed and tested using data from a few outdoor chamber experiments carried out at the California Institute of Technology, but has not been evaluated against the more extensive set of experiments carried out at UNC or SAPRC.

In this paper we describe the development and evaluation of an updated, detailed mechanism for isoprene and its major oxidation products. The mechanism is similar in many respects to the detailed mechanism of Paulson and Seinfeld [15], but incorporates the new product data mentioned above. This mechanism is extensively evaluated using the available environmental chamber data base, with uncertain aspects of the mechanism being adjusted based on results of simulations of these experiments. The chamber data base employed include SAPRC and UNC isoprene - NO_x, methacrolein - NO_x and MVK - NO_x experiments which have not been used previously in any published mechanism evaluations.

The mechanism incorporates the chemical operator formulation employed in the SAPRC-90 [14] and recently updated SAPRC [42] mechanisms. This simplifies the mechanism and reduces the number of reactions required to represent peroxy + peroxy radical reactions, and permits it to be readily incorporated into models using versions of the SAPRC mechanisms. This simplification comes

at the expense of making the mechanism somewhat more approximate in terms of predictions of product yields when NO_x is absent, which includes predictions of peroxy compounds and organic acids. However, the predictions of the mechanisms in the absence of NO_x, even if fully detailed, would be highly uncertain in any case, and cannot be adequately evaluated given the current chamber data base. Therefore, a more detailed mechanism in this respect may not necessarily have more predictive capabilities.

MECHANISM DESCRIPTION

The isoprene and isoprene product reactions are added to the existing updated version of the detailed SAPRC mechanism which has been described elsewhere [14,42,43]. The existing SAPRC mechanism includes explicit representation of the reactions of inorganics, CO, formaldehyde, acetaldehyde, peroxyacetyl nitrate (PAN), propanal, peroxypropionyl nitrate (PPN), glyoxal and its PAN analog, methyl glyoxal, and several other product compounds; uses a "chemical operator" approach to represent peroxy radical reactions; uses generalized reactions with variable rate constants and product yields to represent the primary emitted alkane, alkene, aromatic, and other VOCs (with rate constants and product yields appropriate for the individual compounds); and represents most of the higher molecular weight oxygenated product species using the "surrogate species" approach, where simpler molecules such as propanal or 2-butanone (MEK) are used to represent the reactions of higher molecular weight analogs which are assumed to react similarly.

In the case of isoprene, the previous SAPRC-90 mechanism [14] employed the surrogate species approach to represent reactions of the products of the isoprene reactions which were not incorporated in the existing mechanism. In particular, propanal ("RCHO") was used to represent methacrolein, methyl vinyl ketone, and other products formed in the OH radical reaction, and the overall OH + isoprene reaction was given as [14]

$$OH + ISOPRENE \rightarrow HCHO + RCHO + RO2\text{-}R\cdot + RO2\cdot + C$$

where "RO2-R·" is the chemical "operator" representing the effect of forming peroxy radical intermediates which, in the presence of NO_x, convert NO to NO_2 and generate HO_2 radicals, "RO2·" is the chemical operator used to count the total concentration of peroxy radical species for the purpose of determining the overall rate of peroxy + peroxy radicals, and

"-C" is a "dummy" species used to account for carbon balance when the lumped product species in a reaction have a different number of carbons than the reactants. Note that this one reaction lumps together several rapid consecutive reactions and represents them as a single overall process. The article of Carter [14] should be referred to for a detailed description of the chemical operator method used to represent peroxy radicals in this mechanism; similar approaches are employed in the CB-IV [11,12] and RADM-2 [13] mechanisms.

The chemical operator and rapid consecutive reaction lumping approaches are retained in the isoprene mechanism developed here, but the major oxidation products are represented much more explicitly. Thus, for example, in this mechanism the OH + isoprene reaction shown above is replaced by

$$\begin{aligned}\text{OH + ISOPRENE} \rightarrow\ & 0.088\ \text{RO2-N}\cdot + 0.912\ \text{RO2-R}\cdot + 0.629\ \text{HCHO} \\ & + 0.23\ \text{METHACRO} + 0.32\ \text{MVK} + 0.079\ \text{HOMACR} \\ & + 0.159\ \text{IP-MHY} + 0.079\ \text{IP-HMY} + 0.045\ \text{MEFURAN} \\ & + 0.079\ \text{R2O2}\cdot + 1.079\ \text{RO2}\cdot\end{aligned}$$

(where "HOMACR" refers to hydroxymethacrolein and "IP-HMY" and "IP-MHY refer to the two hydroxy-substituted C_5-unsaturated aldehydes as discussed below). A number of consecutive and competing reactions are lumped together to show the net overall effects of these reactions, both in terms of the distribution of products ultimately formed, the number of extra NO to NO_2 conversions (represented by "R2O2·"), and the total yield of organic nitrates formed by RO_2 + NO reactions (represented by "RO2-N·").

It is important to recognize that while the approximations incorporated in this chemical operator and peroxy radical lumping approach have been shown not to significantly impact ozone predictions [40], this peroxy radical lumping is not designed to accurately predict the distribution of products formed under the very low-NO_x conditions where peroxy + peroxy or peroxy + HO_2 radical reactions dominate. In effect, even the "detailed" mechanism must be considered a condensed mechanism under low-NO_x conditions. To avoid adding a large number of species to the mechanism, the hydroperoxides formed in the peroxy + HO_2 radical reactions are represented by the compounds formed from the peroxy radicals reactions in the presence of NO, together with the lumped structure species "-OOH" to account for the effects on radicals of hydroperoxyde photolyses. The operator approach allows the multitude of peroxy + peroxy radical reactions to be represented in a manner

which avoids the necessity to double (or more) the number of reactions in the mechanism to represent processes which do not affect ozone and are generally otherwise of minor importance. However, it neglects differences among peroxy + peroxy radical rate constants and does not take into account the fact that the distribution of products formed is generally different than those formed when peroxy radicals react in the presence of NO. This limitation, which is also incorporated in the Carbon Bond mechanism [11,12], should be recognized when applying the model to product predictions under low-NO_x or long-range transport conditions. Development of detailed mechanisms which more explicitly represents peroxy + peroxy and hydroperoxide reactions is beyond the scope of this work.

The reactions used to represent the NO_x-air photooxidations of isoprene and its major products in this mechanism are listed in Table 1. Footnotes to the table give the sources or references for the individual reactions, or explain the assumptions or approximations employed. The product species which are represented explicitly are methacrolein, methyl vinyl ketone, two C_5-unsaturated hydroxyaldehydes isomers ("IP-MHY" and "IP-HMY"), glycolaldehyde (hydroxyacetaldehyde), hydroxyacetone, and 3-methylfuran. In addition, separate lumped model species are used to represent the epoxymethyl butenes formed in the $O(^3P)$ and O_3 + isoprene reactions ("ISO-OX"), the nitratoaldehyde products formed from NO_3 + isoprene ("RCHO-NO3"), and the unknown reactive products formed from 3-methylfuran ("HET-UNKN").

A brief summary of the major factors considered when developing this mechanism is given below, together with the uncertain or unknown parameters which were varied or derived from the simulations of the environmental chamber data.

Isoprene + OH Reaction

The various reactions which can occur following the addition of OH radicals to a double bond in isoprene are shown in Figure 1. Quite a few reaction routes are possible because (1) the OH can add to four different positions in isoprene (2-methyl-1,3-butadiene), (2) the allylic radicals formed have two radical centers, which can yield two different peroxy radicals when they react with O_2, and (3) the alkoxy radicals with δ-hydrogens can react via 1,5-H shift isomerization *only* if the abstractable hydrogen is in a *cis*- orientation relative to the radical center. Because of these considerations, a total of 12 overall processes could occur in the OH + isoprene system, giving rise to differing products or (in some cases) differing amounts of NO converted to NO_2 in the process. This does not include

nitrate formation from the peroxy + NO reactions, which is not shown on Figure 1, but which is non-negligible as discussed below.

The experimentally measured product yields which we use in the mechanism are: methacrolein, 23%; methyl vinyl ketone, 32%, formaldehyde, 60 ± 10%, and 3-methylfuran, 4.5%. These are based on the reported data of Atkinson *et al*. [29], Tuazon and Atkinson [30], Paulson *et al*. [27] and Miyoshi *et al*. [31]. The methacrolein, methyl vinyl ketone and 3-methylfuran data of Paulson *et al*. [27] were corrected for $O(^3P)$ atom reaction using an estimated $O(^3P)$ atom reaction rate constant with isoprene which was a factor of 1.5-1.6 higher than the measured value [28], while the data reported by Atkinson *et al*. [29] and Tuazon and Atkinson [30] were not corrected for $O(^3P)$ atom reaction with isoprene. This correction is estimated to increase the measured yields of methacrolein, methyl vinyl ketone, HCHO and 3-methylfuran [29,30] by ~8%, resulting in product formation yields in excellent agreement with those of Miyoshi *et al*. [31] and with the average of the reported product yields of Tuazon and Atkinson [30], Paulson *et al*. [27] and Miyoshi *et al*. [31]. The data of Miyoshi *et al*. [31] were corrected for $O(^3P)$ atom reaction with isoprene using a rate constant similar to that measured by Paulson *et al*. [28].

Product analysis of the OH radical reaction with isoprene and isoprene-d_8 in the presence of NO, using atmospheric pressure ionization tandem mass spectrometry (API-MS), has shown the formation of unsaturated C_5-hydroxycarbonyls such as $HOCH_2C(CH_3)=CHCHO$ and $HOCH_2CH=C(CH_3)CHO$ and C_4-hydroxycarbonyls of formula $C_4H_6O_2$, such as hydroxymethacrolein [$CH_2=C(CHO)CH_2OH$] [32]. These API-MS analyses showed no evidence for the formation of C_5-dihydroxycarbonyls [32]. Results of derivitization with subsequent GC-MS product analyses in isoprene - NO_x - air environmental chamber experiments by Yu *et al*. [33] are consistent with the API-MS data [32] in that unsaturated C_5-hydroxycarbonyls and C_4-hydroxycarbonyls are observed, but not C_5-dihydroxycarbonyls. Accordingly, based largely on these data [32] and the FT-IR spectroscopic evidence of Tuazon and Atkinson [30] for the formation of carbonyls other than methacrolein and methyl vinyl ketone, we include the formation of hydroxymethacrolein [$CH_2=C(CHO)CH_2OH$] and the C_5-hydroxyaldehydes $HOCH_2C(CH_3)=CHCHO$ and $HOCH_2CH=C(CH_3)CHO$ as products of the OH radical-initiated reaction of isoprene in the presence of NO, but we assume that the formation of dihydroxycarbonyls (for example, $HCOCH=C(CH_2OH)_2$ and $HOCH_2CH=C(CH_2OH)CHO$, which might be formed by pathways "D" and "E" on Figure 1) is negligible. This mechanism predicts that the formation yield of formaldehyde should be the sum of the formation yields of methacrolein, methyl

vinyl ketone and hydroxymethacrolein, and this is consistent with the experimentally measured HCHO yields of Tuazon and Atkinson [30] and Miyoshi *et al*. [31].

The scheme in Figure 1 does not include organic nitrate formation from peroxy + NO reactions [60], as shown, for example:

$$HOCH_2CH=C(CH_3)CH_2OO\cdot + NO \xrightarrow{M} HOCH_2CH=C(CH_3)CH_2ONO_2$$

Organic nitrate IR bands were observed by Tuazon and Atkinson [30] and, based on an assumed infrared absorption cross-section(s), these nitrate products were estimated to account for ~8-13% of the overall reaction products [30]. This reaction pathway occurs in the NO_x - air oxidations of alkanes, becoming relatively more important as the size of the molecule increases [60]. We estimate that the likely range for the organic nitrate formation yield in the OH + isoprene reaction in the presence of NO is 6-12%, but because of its importance in affecting isoprene reactivity predictions (see below), the organic nitrate yield is used as an adjustable parameter in the model simulations of the isoprene experiments.

Isoprene + O_3 Reaction

The isoprene + O_3 reaction mechanism we use is based on the product data obtained by Atkinson *et al*. [16] and Aschmann and Atkinson [18] and the mechanism discussed by Aschmann and Atkinson [18]. The reaction is assumed to proceed via six overall reaction routes [18]:

ISOPRENE + O_3

→ 1,2-ozonide

→ HCHO + $[CH_2=CH\cdot C(CH_3)OO\cdot]^*$ A (20%)

→ $[H\cdot CHOO\cdot]^*$ + CH_3-CO-CH=CH_2 B (16%)

→ 1,2-epoxy-2-methyl-3-butene + O_2 C (4%)

→ 3,4-ozonide

→ HCHO + $[CH_2=C(CH_3)\cdot CHOO\cdot]^*$ D (20%)

→ $[H\cdot CHOO\cdot]^*$ + $CH_2=C(CH_3)CHO$ E (39%)

→ 1,2-epoxy-3-methyl-3-butene + O_2 F (1%)

The $[CH_2=CH\cdot C(CH_3)OO\cdot]^*$ biradical formed in pathway (A) is assumed to react via the hydroperoxide channel, resulting in near unit yields of OH radicals [18,24]:

$$[CH_2=CH\cdot C(CH_3)OO\cdot]^* \rightarrow [CH_2=CHC(OOH)=CH_2]^* \rightarrow CH_2=CHC(O)\dot{C}H_2 + OH$$
$$CH_2=CHC(O)\dot{C}H_2 + O_2 \rightarrow CH_2=CHC(O)CH_2OO\cdot$$
$$CH_2=CHC(O)CH_2OO\cdot \xrightarrow[-NO_2]{NO} CH_2=CHC(O)CH_2O\cdot \rightarrow CH_2=CH\dot{C}O + HCHO$$

The $[CH_2=C(CH_3)\cdot CHOO\cdot]^*$ biradical formed in pathway (D) cannot rearrange to form the hydroperoxide, with subsequent decomposition to form the OH radical, nor are there other obvious facile radical fragmentation reactions. Paulson *et al*. [34] observed the formation of propene in ~7% yield in the isoprene + O_3 reaction, while Aschmann and Atkinson (unpublished data, 1995) obtain a propene formation yield of ~4.3%. Propene formation is attributed to the $[CH_2=C(CH_3)\cdot CHOO\cdot]^*$ biradical rearranging and decomposing to propene + CO_2 (see [24] and references therein). We assume that 75% of this biradical is stabilized to form an unspecified product with similar reactivity as an aldehyde, and the other 25% decomposes to form propene + CO_2. This predicts a propene yield from the isoprene + O_3 reaction of 5%, within the range of uncertainty of the data of Paulson *et al*. [34] and the unpublished data of Aschmann and Atkinson (1995).

The relative importance of pathways (A) and (D) were derived as discussed by Aschmann and Atkinson [18].

Isoprene + $O(^3P)$ Reaction

Although this reaction is probably unimportant under most ambient conditions, it occurs to a non-negligible extent in isoprene - NO_x - air chamber runs, and the $O(^3P)$ + isoprene mechanism assumed affects the value of the organic nitrate yield in the OH reaction which best fits the data. By modeling product formation in outdoor NO_x - isoprene - air chamber runs, Paulson *et al*. [27] concluded that this reaction forms epoxides in 85 ± 9% yield and that fragmentation to radicals accounts for 8 ± 3% of the overall reaction. Approximately 14% of C_5-aldehyde and unidentified product formation was also observed [27].

The experiments modeled in this study are sensitive to the radical yields from this reaction, and this is used as an adjustable parameter (see below). Formation of ~75-90% (epoxide + aldehyde) products is consistent with previous product studies of $O(^3P)$ atom reactions with $\geq C_3$ alkenes and 1,3-butadiene [61-63], and hence the radical yield from the isoprene reaction is restricted to a 10%-25% range. Fragmentation is assumed to occur via $\cdot CH_2C(O\cdot)(CH_3)CH=CH_2 \rightarrow CH_3\cdot + \cdot CH_2C(O)CH=CH_2$, with the alkoxy radical formed from the $\cdot CH_2C(O)CH=CH_2$ radical after O_2 addition and NO to NO_2 conversion decomposing to yield HCHO + $CH_2=CH\dot{C}O$.

Isoprene + NO_3 Reaction

This reaction is expected to be an important sink for isoprene at nighttime, and its mechanism also has a significant effect on model simulations in isoprene - NO_x - air chamber runs. The reaction proceed by initial addition to the >C=C< bonds, with initial addition to the 1-position dominating over addition to the 4-position by a factor of ~3.5 [35]. Under laboratory conditions, peroxy + peroxy and peroxy + HO_2 radical reactions dominate. Using *in situ* FT-IR spectroscopy, Skov *et al*. [35] concluded that the major product formed is $O_2NOCH_2C(CH_3)=CHCHO$ together with minor amounts of the nitratocarbonyls $O_2NOCH_2CH=C(CH_3)CHO$ and $CH_2=C(CH_3)C(O)CH_2ONO_2$ and the hydroxynitrates $HOCH_2CH=C(CH_3)CH_2ONO_2$ and $CH_2=C(CH_3)CH(OH)CH_2ONO_2$. Recently, Kwok *et al*. [36], using API-MS analyses, observed the formation of C_5-nitratocarbonyls such as $O_2NOCH_2C(CH_3)=CHCHO$, C_5-hydroxynitrates such as $HOCH_2CH=C(CH_3)CH_2ONO_2$, C_5-nitratohydroperoxides such as $O_2NOCH_2C(CH_3)=CHCH_2OOH$, and C_5-hydroxycarbonyls identical or analogous to those formed from the OH radical reaction in the presence of NO [32]. Fragmentation of the intermediate alkoxy radicals to methacrolein and methyl vinyl ketone is minor, with methacrolein and methyl vinyl ketone yields of 3.5 ± 1.4% each being measured by Kwok *et al*. [36].

Consistent with these data, we assume that the NO_3 + isoprene involves primarily formation of $\cdot OOCH_2CH=C(CH_3)CH_2ONO_2$, which in the presence of NO forms the corresponding alkoxy radical. This alkoxy radical could react with O_2 forming HO_2 and $CH_3C(CH_2ONO_2)=CHCHO$, isomerize by H-atom abstraction from the $-CH_2ONO_2$ group,

$$\cdot OCH_2CH=C(CH_3)CH_2ONO_2 \rightarrow HOCH_2CH=C(CH_3)CH(\cdot)ONO_2 \rightarrow HOCH_2CH=C(CH_3)CHO + NO_2$$

or isomerize by H-atom abstraction from the $-CH_3$ group,

$$\cdot OCH_2CH=C(CH_3)CH_2ONO_2 \rightarrow [\ HOCH_2CH=C(CH_2\cdot)CH_2ONO_2 \leftrightarrow HOCH_2CH(\cdot)C(=CH_2)CHO\ ]$$

giving rise to C_5-hydroxynitratocarbonyls or formaldehyde plus a C_4-nitratocarbonyl through reactions analogous to those shown in Figure 1 for the OH radical reaction system. The products formed in the O_2 reaction and the isomerization involving abstraction from the $-CH_2ONO_2$ group are consistent with the product data of Kwok *et al.* [36] discussed above, but Kwok *et al*. [36] did not observe the formation of C_5-hydroxynitratocarbonyls nor C_4-nitratocarbonyls expected to arise after isomerization involving abstraction from the $-CH_3$ group. Based on qualitative estimates of the relative amounts of

products seen in the system of Kwok *et al.* [36], we assume that $HOCH_2CH=C(CH_3)CHO + NO_2$ formation occurs ~20% of the time, and the remainder of the reaction pathways are represented by $CH_3C(CH_2ONO_2)=CHCHO + HO_2$. This is highly uncertain.

Reactions of Methacrolein and Methyl Vinyl Ketone

The mechanisms used for the reactions of methacrolein and methyl vinyl ketone are documented in the footnotes to Table 1. The rate constants for the reactions of methacrolein and methyl vinyl ketone with OH radicals [24], O_3 [24] and NO_3 radicals [36] appear to be reliably known. The products and mechanism of the OH radical reactions in the presence of NO appear to be reasonably well understood [37,38], with the available product data accounting for essentially all of the reaction routes (see footnotes 11 and 17).

No reaction of the NO_3 radical with methyl vinyl ketone has been observed [36] (with only an upper limit to the rate constant being available [36]), and the NO_3 radical is assumed to react with methacrolein by both H-atom abstraction from the -CHO group and NO_3 radical addition to the >C=C< bond [24,36], and a 50% contribution by both reaction pathways is assumed here [see footnote 16]. The mechanism of the NO_3 radical addition reaction is uncertain because it is not known whether the $CH_2(ONO_2)C(O\cdot)(CH_3)CHO$ decomposes to form $H\dot{C}O + CH_3C(O)CH_2ONO_2$ (which is assumed in this mechanism) or $HCHO + NO_2 + CH_3C(O)CHO$. This determines how the NO_3 radical reaction with methacrolein affects radicals and NO_x in the system, although it does not have a large effect on the results of the chamber simulations.

The OH radical formation yields from the reactions of O_3 with methacrolein and methyl vinyl ketone have been measured to be 20^{+10}_{-13}% and 16±8%, respectively [45]. The formaldehyde and methylglyoxal yields observed by Grosjean *et al.* [44] indicate that the ozonides decompose primarily to form $[HCHO_2]^*$ and methylglyoxal, with this route occurring between 60-95% of the time for methacrolein and 80-95% of the time for MVK. We assume that $[HCHO_2]^*$ + methylglyoxal formation occurs 90% of the time in the methacrolein reaction and 95% of the time from MVK, as indicated by the data of Grosjean *et al.* [44]. Therefore, since the OH yield from $[HCHO_2]^*$ is expected to be 12% [24], OH yields of ~100% from $[HCOC\cdot(CH_3)OO\cdot]^*$ and $[CH_3COCH\cdot OO\cdot]^*$ would account for the measured overall OH yields from the O_3 + methacrolein and MVK reactions. 100% OH radical formation from $[HCOC(CH_3)\cdot OO\cdot]^*$ is expected to occur via H-shift isomerization to an excited hydroperoxide which subsequently decomposes to form OH and other radical products in

a manner analogous to that shown for [CH_2=CH·C(CH_3)OO·]*, above. Radical formation from [CH_3COCH·OO·]* is expected to occur via interconversion to [HCOC(CH_3)·OO·]* via a primary ozonide intermediate, as discussed in Footnote 18 to Table 1.

Methacrolein and methyl vinyl ketone have significant absorption cross-sections in the 300-400 nm region [47], and thus their photodecomposition in the atmosphere could be important if their quantum yields were sufficiently high. Methacrolein and MVK photolyses were studied recently by Raber and Moortgat [47], who observed that, like acrolein [46], photodecomposition under atmospheric conditions is highly inefficient for these compounds. The overall photodecomposition quantum yields, using a light source covering the ~270-380 nm region, were determined to be ≤0.05 for methacrolein and ~0.02-0.05 for MVK [47]. These values are uncertain because of the low conversion of the starting material in the experiments. No information was obtained about the wavelength dependence of the quantum yields. Since it is expected that if quantum yields decrease with wavelength (if they have any wavelength dependence), and since the light employed by Raber and Moortgat [47] had significant intensity at wavelengths lower than the <300 nm atmospheric cutoff, one should consider these overall quantum yields to be upper limits of the effective atmospheric values. Because of this, the effective overall quantum yields for the photodecompositions of these compounds were treated as adjustable parameters in our simulations of the environmental chamber data.

Raber and Moortgat [47] were able to fit their product data for MVK using a mechanism assuming 70% decomposition to propene + CO, with the remainder fragmenting as discussed in Footnote 19 to Table 1. They did not attempt to develop a mechanism for the photodecomposition of methacrolein because of difficulties in assessing the origin of the observed products and lack of needed kinetic data. For this work, we derived an assumed mechanism by analogy with mechanism derived by Gardner *et al*. [46] to fit their photodecomposition data for acrolein in synthetic air (see footnote 15 to Table 1).

The absorption cross-sections for methacrolein and MVK are very similar to each other [47] and to that of acrolein [46]. Because the general mechanism already uses the acrolein absorption cross-section to represent unknown photoreactive aromatic products [42,43], these values, which are tabulated in Table 2, are also used for these isoprene products. Any small differences between the acrolein cross-sections used in our mechanism and the actual values for methacrolein and MVK would

be compensated for when the effective overall quantum yields are derived by adjustment to fit the environmental chamber data.

Reactions of Other Unsaturated Aldehyde Products

As discussed above and shown in Figure 1, the reactions of isoprene with the OH radical and the NO_3 radical lead to a number of unsaturated carbonyl products in addition to methacrolein and methyl vinyl ketone, including hydroxymethacrolein ("HOMACR") and the C_5-hydroxyaldehydes $HOCH_2CH=C(CH_3)CHO$ ("IP-MHY") and $HOCH_2C(CH_3)=CHCHO$ ("IP-MHY"). Hydroxymethacrolein is assumed to react with an analogous mechanism to methacrolein, except as indicated in the footnotes to Table 1, and with the OH radical addition rate constant being a factor of 1.6 higher than that for methacrolein [51]. The mechanisms and rate constants for the C_5-hydroxyaldehydes are estimated as discussed in Footnotes (23-29). Generally their mechanisms are assumed to be analogous that used for methacrolein. For example, they are assumed to have the same photodecomposition quantum yields as determined by model simulations of the methacrolein - NO_x - air runs, and the OH yields formed in the -CHO substituted Criegee biradicals are assumed to be the same as assumed in the methacrolein system. As indicated in footnotes 23. 25, and 28, they are estimated to react more rapidly with OH radicals, NO_3 radicals and O_3 because of the greater degree of substitution about the double bond. All the C_5 isomers are assumed to react with the same rate constants and analogous mechanisms, though the product distributions differ and in most cases are represented explicitly. The major exceptions are that $HOCH_2COCHO$ is represented by methylglyoxal, and $HOCH_2COCH_2OH$ is represented by hydroxyacetone. These are relatively minor secondary products and are not expected to have greatly different effects on the system than the compounds used to represent them.

Reactions of Other Products

The other observed or expected primary isoprene reaction products are 3-methylfuran from the OH reaction, isoprene epoxides from the O_3 and $O(^3P)$ reactions, and unsaturated nitratoaldehydes from the NO_3 reaction. The expected secondary products which are treated explicitly in this mechanism are methyl glyoxal, glycolaldehyde, hydroxyacetone, and glyoxal. In addition, some minor products were represented by lumped aldehyde ("RCHO") and ketone ("MEK") species as indicated in the footnotes to Table 1. The mechanisms used for these explicit or lumped product species are given in the table, with footnotes documenting the rate constants and reactions assumed. Note that the mechanism used for the minor product 3-methylfuran is a highly parameterized representation based on a parameterized

model for furan used to fit results of furan - NO_x - air chamber experiments [53] (see also footnote 32). None of these mechanisms were adjusted in the model simulations discussed in this work.

ENVIRONMENTAL CHAMBER EVALUATION

Chamber Runs Employed

Data from a total of 28 isoprene - NO_x - air, 15 methacrolein - NO_x - air, and 11 methyl vinyl ketone - NO_x - air environmental chamber experiments, obtained using seven different chambers at two different laboratories, were used in the development and evaluation of the mechanism discussed here. The major characteristics of the chambers employed, and references where more details can be obtained concerning the chambers and experimental procedures, are summarized in Table 3, and Table 4 summarizes the initial reactant concentrations used in these experiments. These runs consist of all the UNC and SAPRC experiments used in the evaluation of the SAPRC-90 and RADM-2 mechanisms [40,41], and most of those used in the development of CB-IV [11,12]. In addition, they include more recent experiments at UNC and SAPRC which have not been used for previous mechanism evaluations. The new SAPRC experiments include outdoor runs in which the spectral distribution was monitored periodically during the runs, and runs in a new Teflon chamber with a xenon-arc light source (Table 3). The new UNC experiments were carried out in 1992 and 1993 and are believed to have high quality methacrolein and methyl vinyl ketone data (H. E. Jeffries, private communication, 1995). These new UNC experiments include one divided chamber run each with methacrolein and methyl vinyl ketone. In addition, one of the new UNC isoprene experiments includes data for methyl glyoxal, glycolaldehyde, and hydroxyacetone as measured by DNPH [68,69]. Although Jeffries (private communication) estimates these DNPH data may have uncertainties of up to 50%, they provide the first data available to test model predictions for these secondary products. The experimental procedures for the earlier (1980-1981) UNC experiments are documented by Jeffries *et al.* [66,67]. The SAPRC indoor experiments are described by Carter *et al.* [39], and the procedures employed for the SAPRC outdoor experiments used in this work are discussed by Carter *et al.* [65].

Because of the uncertainties in chamber effects and (in some cases) characterization of chamber conditions (see, for example, [40,41]), the use of data from different chambers with different operating procedures for the evaluation of a chemical mechanism reduces the probability that errors in the chamber characterization assumptions compensate for errors in the mechanism [70]. Chamber

effects are influenced by the type of chamber surface, humidity, and temperature [39-41,65]. The SAPRC EC has a different interior surface than the other chambers, the level of humidification and purification of the air employed differs among the various chambers (see Table 3), and the outdoor chamber experiments are carried out over a range of temperature.

The use of differing light sources also allows for a more comprehensive mechanism evaluation, especially for mechanisms (such as this) which involve photoreactive species with uncertain quantum yields. The data set used here includes experiments using blacklights, xenon arc lights, and sunlight. Blacklights give a good representation of solar light in the UV region, but not in the higher wavelength region where the photolysis of α-dicarbonyl and (to a lesser extent) unsaturated carbonyl products occurs. Xenon arc lights give the best representation of sunlight possible with artificial lights, although the match of the xenon arc spectrum with that of solar radiation is not exact [65]. In particular, the match of the xenon arc spectrum with that of solar radiation at the lowest wavelength depends on the quality of the spectral filter used with the xenon arc light source. During the time the EC runs in this set were conducted, the short wavelength ($\lambda \leq 320$ nm) intensity of the filtered light source for that chamber was much lower than that of sunlight because of solarization of the Pyrex filter employed, and perhaps other factors [39]. In contrast, the $\lambda \leq 300$ nm intensity of the xenon arc lights used with the XTC was somewhat higher than ambient sunlight [39,65]. Outdoor chambers obviously have the most realistic light source, although the light intensity and spectral distribution are variable and intrinsically difficult to characterize. Furthermore, the transmission characteristics of the chamber walls also have to be taken into account [39,65,71].

Table 4 also indicates the experiments used for adjusting uncertain parameters in the mechanism development. Certain experiments were excluded for this purpose because the fits of model simulations to the experimental data for these runs were inconsistent with the trends observed for other runs, suggesting experimental problems, and these runs are indicated in footnotes to Table 4. For these runs. no adjustment of the uncertain parameters could change the nature of the model fits to those runs relative to the other runs, so it was decided that including them in the optimizations would bias the results. In addition, as discussed by Carter *et al.* [39], the SAPRC EC had problems around the time of the runs in the EC-600's, so we considered it prudent not to use these chamber experiments in the optimizations.

Outdoor chamber runs were not used in the optimizations for two reasons. First, the conditions of outdoor chamber experiments are more difficult to characterize because of the variable light intensity, spectral distribution, and other conditions. In addition, it is useful to reserve a set of runs, not used in the mechanism optimization, for an independent evaluation of the mechanism. Outdoor runs, which in some respects more closely represent ambient conditions, are perhaps most appropriate for this purpose. This was the approach employed in the evaluation of the SAPRC-90 [41] and RADM-2 [40] mechanisms.

Chamber Characterization Model

Testing of chemical mechanisms against environmental chamber results requires including appropriate representations of chamber-dependent effects such as wall reactions and characteristics of the light source. The methods used in this study are based on those discussed in detail by Carter and Lurmann [40,41], a detailed discussion of which is beyond the scope of this paper. For the SAPRC runs, the parameters, particularly those involving the chamber radical source [72], were re-evaluated and modified as discussed by Carter *et al.* [65]. The primary change between these two studies [65,72] was that the magnitudes of the chamber radical source were reduced to a significant extent for the Teflon Chamber (ITC) runs and, to a lesser extent, for the EC runs based on indications that deriving the radical source by modeling *n*-butane - NO_x - air experiments gave more consistent results than modeling the radical tracer - NO_x - air experiments used previously [40,41,72]. The chamber-dependent parameters for modeling the UNC chamber runs were the same as employed previously [40,41], except that ~3 ppb HONO was assumed to be initially present, based on the recommendations of the UNC researchers for modeling the runs conducted during the 1992-1993 time period (Sexton and Jeffries, private communication, 1995).

The photolysis rates for the indoor chamber runs were derived from the measured NO_2 photolysis rates (k_1), combined with measured spectra of the blacklight or xenon arc light sources [39,65]. For the SAPRC outdoor runs, spectral measurements were made during the course of the experiments to characterize the light spectra and intensity, with corrections made for effects of transmissions and reflections through the Teflon walls [65]. Only clear sky OTC runs are modeled here. For the UNC experiments, the in-chamber spectral fluxes were derived at 20 minute intervals during the run by Jeffries and co-workers as discussed by Carter and Lurmann [40], using a model developed and evaluated for this purpose [71].

Optimization of Methacrolein and Methyl Vinyl Ketone Mechanisms

Figures 2-4 show fits of model simulations to ozone formation and NO oxidation rates (Figure 2), to rates of methacrolein or MVK consumption (Figure 3), and to PAN formation (Figure 4) for all the runs with these compounds modeled in this study. Note that the ability of the model to simulate NO oxidation and O_3 formation is assessed by comparing experimental and calculated values of $\{[O_3]_t-[O_3]_{init})-([NO]_t-[NO]_{init}\}$, which we designate $d(O_3-NO)$ [42,73]. As discussed elsewhere [40,41,74,75], this gives a direct measure of the amount of conversion of NO to NO_2 by peroxy radicals formed in the photooxidation reactions, which is the process directly responsible for ozone formation in the atmosphere. This parameter $\{[O_3]_t-[O_3]_{init})-([NO]_t-[NO]_{init}\}$ is useful for assessing model performance under both high-NO and high-O_3 conditions. The dotted lines show results of model simulations if it is assumed that photodecomposition of both methacrolein and methyl vinyl ketone are negligible. The solid lines show the results of the model simulations with the overall quantum yields for methacrolein or methyl vinyl ketone photolyses being adjusted to minimize the least-squares discrepancies between the calculated and experimental values of $d(O_3-NO)$, PAN, and methacrolein, or methyl vinyl ketone, for the runs used in the optimizations.

Figures 2-4 indicate that it is necessary to assume a non-negligible photodecomposition of methacrolein for the model to adequately predict the $d(O_3-NO)$ formation and methacrolein consumption rates in the blacklight, XTC, and OTC chamber runs. However, the model is relatively insensitive to methacrolein photolysis in the simulations of the EC and the UNC runs, at least if methacrolein is assumed to have quantum yields no higher than those which fit the runs in the other chambers. One reason for the lower sensitivity in the EC and UNC runs might be that these chambers have somewhat higher chamber radical sources than the SAPRC Teflon chambers [39-41,65,72], resulting in runs in these chambers being less sensitive to radical initiation processes in the gas-phase chemistry. In addition, as indicated above, the light source for the EC chamber during the period of these experiments was relatively low in UV intensity, compared to the other chambers. In the case of the UNC chamber, the lower sensitivity may also be attributed, at least in part, to the runs being initiated by early-morning sunlight, when UV intensity is extremely low. The SAPRC OTC experiments are initiated much later in the morning, when the UV intensity is approaching its full mid-day level. The results for methyl vinyl ketone are similar to those for methacrolein, except that all of the experiments are less sensitive to methyl vinyl ketone photodecomposition.

The best fits are obtained using wavelength-independent photodecomposition yields of 0.0036 for methacrolein and 0.011 for MVK. These are not inconsistent with the data of Raber and Moortgat [47], who obtained photodissociation quantum yields of ≤0.05 and 0.02-0.05, respectively, using a light source with much greater relative UV intensity. One would expect these photodecompositions to have some wavelength dependence, and lower quantum yields for atmospheric conditions than those derived by Raber and Moortgat [47] is not unexpected. The fact that reasonably good fits are obtained in experiments using a variety of light sources indicates that assuming the wavelength independent quantum yields derived in this work should probably give satisfactory results in simulating range of lighting conditions which may occur in the atmosphere. However, quantum yields derived using light sources much richer in the UV may result in overestimation of atmospheric photolysis rates, at least for highly inefficient photodecompositions such as these.

We have no data for deriving the photodecomposition rates for hydroxymethacrolein, or the two C_5-unsaturated hydroxyaldehyde isomers. Since the expected photoreactive regions of these molecules are similar to that for methacrolein, we assume they all have the same absorption cross-sections and quantum yields as methacrolein.

Optimization of Isoprene Mechanism

In order to obtain satisfactory fits of the chamber data and model predictions, either y^{OH}_{RNO3}, the organic nitrate yield in the OH radical reaction, or y^{O}_{Rad}, the radical yield in the $O(^3P)$ atom reaction, had to be adjusted. The effects of adjusting other uncertain parameters, such as the rate constant(s) for the reactions of O_3 with the C_5-unsaturated hydroxyaldehydes and the radical yield in the NO_3 radical reaction, were also examined, and it was found that adjusting y^{OH}_{RNO3} or y^{O}_{Rad} dominated the effects of adjusting these other parameters. Therefore, it was decided not to modify the other parameters from their initially estimated values.

Because the parameters y^{OH}_{RNO3} and y^{O}_{Rad} both affect radical initiation/termination processes, the best fit value of one of these parameters depends on the assumed value for the other. For example, if y^{O}_{Rad} is held at its maximum value of 25%, then the $d(O_3\text{-NO})$ data in the isoprene runs are best fit assuming y^{OH}_{RNO3} of 8.8%, while if the minimum y^{O}_{Rad} value of 10% is assumed, the best fit y^{OH}_{RNO3} is 4.9%. If both are optimized simultaneously, the best fits are obtained with y^{O}_{Rad} = 30% and y^{OH}_{RNO3} of 10%. Since the y^{O}_{Rad} obtained if both are optimized is slightly outside of our estimated uncertainty range, this set is not used in the model. However, if we use the set with the highest value of y^{O}_{Rad}

consistent with our uncertainty range (i.e., 25%), then the sum of squares error in the fits to d(O_3-NO) is only ~6% higher than the optimum. On the other hand, using the set with y^{O}_{Rad} at the low end of the uncertainty range gives a sum of squares error about twice that of the optimum. For that reason, we use the set based on assuming the highest acceptable value of y^{O}_{Rad} for the final mechanism. Note that the corresponding value of y^{OH}_{RNO3} (8.8%) is near the middle of our estimated uncertainty range of 6-12% for this parameter. However, considering the uncertainties in characterizing the chamber data and the other uncertainties in the mechanism, the chamber data must be considered to be probably inadequate to uniquely determine both these parameters, whose values therefore must be considered to be uncertain. However, if a value of one is assumed (or becomes known), then the chamber data, which are highly sensitive to their relative values, constrains the other reasonably tightly.

Model Performance in Simulations of the Isoprene Experiments

Figures 5-8 show experimental and calculated concentration-time profiles for d(O_3-NO), methacrolein, MVK, PAN, and formaldehyde. Plots for the organic products are not shown for runs where there are no experimental data for the compound, or for runs where the data are considered to be anomalous or unreliable. The latter include PAN in the SAPRC ETC, DTC and OTC runs and formaldehyde in the EC and ITC runs, which are considered to be unreliable for reasons discussed by Carter *et al.* [39]. The methacrolein and methyl vinyl ketone data in the earlier UNC runs are not plotted because they appear to be anomalous and because the data from the more recent UNC runs are considered to be of much higher quality (Jeffries, personal communication, 1995).

Figure 5 shows that with a few exceptions the model gives quite good fits to d(O_3-NO) in most of the SAPRC and UNC isoprene experiments. The model underpredicts O_3 in runs ITC811 and ITC812, but does not show this discrepancy in the simulations of the other blacklight chamber runs. (The reason for the underprediction of d(O_3-NO) in runs ITC811 and (especially) ITC812 is not known, and correspondingly poor fits are observed in simulations of most of the other species. The conditions of these runs are apparently not well characterized in the model.) The model gives good fits to the d(O_3-NO) in all the xenon arc chamber runs except for run EC669, which was carried out around a time when the light source was undergoing unexplained spectral changes [39]. The fits to the UNC outdoor runs are also quite good, except for the period following the first O_3 maximum in the July 16, 1980 experiments. For some reason, the model tended to underpredict the initial rate of NO oxidation in the earlier UNC experiments, and overpredict it in the later ones. Thus, while some discrepancies and apparently anomalous experiments are observed, the results of these simulations,

taken as a whole, do not indicate the existence of systematic discrepancies in d(O_3-NO) predictions which would signal errors or biases in the mechanism. While the possibility of mechanism errors certainly cannot be ruled out, particularly in aspects to which these chamber simulations are not highly sensitive, the model performance in the simulations of this highly varied set of experiments suggest that the discrepancies observed are more likely due to data, chamber, or run characterization problems than to major errors in the mechanism.

Figures 6 and 7 show that the model gives reasonably good simulations of the methacrolein and methyl vinyl ketone profiles except for ITC811 and ITC812, and except for methyl vinyl ketone in the EC experiments. Underprediction of methacrolein and methyl vinyl ketone in ITC811 and ITC812 is consistent with the observation that d(O_3-NO) is also underpredicted in these runs. We suspect that the underprediction of methyl vinyl ketone in the EC runs is due to calibration problems for this compound at the time these experiments were conducted, since methyl vinyl ketone is well fit for other experiments carried out at different times at SAPRC, as well as for those carried out at UNC. The reasonably good simulations of the decay rates of these products at the end of the runs is consistent with the generally good simulations of the decays of these compounds in the experiments where they are the reactant, as shown in Figure 3.

The one definite area of systematic discrepancy observed in this evaluation is the simulations of PAN in the isoprene experiments. This is shown in Figure 8, which indicates an underprediction of PAN by an average of ~40% in the experiments where the model gave good fits to d(O_3-NO). (The good PAN fit for run EC669 is probably due to compensating errors, since the model overpredicts the final O_3 (see Figure 3), and since O_3 and PAN tend to be correlated.) In contrast, Figure 4 shows that PAN is reasonably well simulated in most of the methacrolein and methyl vinyl ketone experiments. Either there is some PAN formation process(es) in the reactions of the other isoprene products or in the isoprene + O_3 reaction which is not well represented in this model, or there is a product formed in the isoprene - NO_x - air irradiations which co-elutes with PAN on the GC columns used at both SAPRC and UNC. The co-eluting PAN species is clearly not MA-PAN, since separate peaks attributable to that compound are seen in the SAPRC (unpublished data) and UNC (Jeffries, private communication, 1995) methacrolein - NO_x experiments.

Figure 9 shows that the model performs reasonably in simulating the formaldehyde in the more recent UNC experiments, but overpredicts formaldehyde formation in the recent SAPRC runs.

(The model also overpredicts formaldehyde in earlier SAPRC runs, but these data are considered unreliable for reasons discussed by Carter *et al.* [39].) The formaldehyde instrument used in the more recent SAPRC runs tended to give high formaldehyde values (compared to model predictions) in propene - NO_x - air and other experiments [39, unpublished results from this laboratory], so the possibility that the poor fits for these runs may be due to analytical problems cannot be ruled out. Until this is verified and the reasonably good fits for the UNC runs are confirmed in simulations of data from other laboratories, we consider the present data set inadequate to evaluate this aspect of the isoprene mechanism.

One of the new UNC experiments provided to us by Jeffries and co-workers (private communication, 1995) (JN1793R) had concentration-time data for methylglyoxal, hydroxyacetone, and glycolaldehyde, measured by DNPH [68,69]. Jeffries (private communication, 1995) considers these data to be uncertain by up to ~±50% due to baseline variation and other problems, so this should be taken into account when interpreting simulations of these data. An indication of the performance of this method can be obtained by comparing the simultaneous DNPH and GC-FID measurements of methacrolein (Figure 6) and MVK (Figure 7) made during this experiment, where it can be seen that the DNPH data agree very well with the more reliable GC-FID data for methacrolein, but that the agreement for MEK is only within a factor of ~2.

The experimental and calculated profiles for those species in that run are shown on Figure 10. Although there are some apparently anomalous hydroxyacetone points (two points rejected by the UNC researchers are not shown), and the model tends to somewhat overpredict glycolaldehyde and underpredict methyl glyoxal, the fits are remarkably good considering the uncertainties in the DNPH measurement technique. If the underprediction of methylglyoxal is real, it might be related to the apparent underprediction of PAN in the isoprene experiments, since methylglyoxal undergoes rapid photolysis, primarily to form PAN. However, it is difficult to make definitive conclusions based on simulations of a single experiment.

Performance of the 1992 Paulson and Seinfeld Mechanism

Figure 5 also shows the results of model simulations of the isoprene - NO_x - air chamber experiments using the mechanism of Paulson and Seinfeld [15], which was the most up-to-date detailed mechanism for isoprene prior to this work. It can be seen that, although the mechanisms have much in common concerning major aspects of the isoprene reaction system, the Paulson and Seinfeld

[15] mechanism is substantially different in simulations of most of the chamber experiments, tending to significantly underpredict ozone formation and NO oxidation rates in almost all cases. This is also the case for all but one of the SAPRC outdoor chamber (OTC) experiments, which is somewhat surprising because that chamber is very similar to the California Institute of Technology chamber used by Paulson and Seinfeld [15] to evaluate their mechanism. The Paulson and Seinfeld mechanism [15] also underpredicts d(O_3-NO) formation rates in most of the UNC outdoor chamber experiments, though in some high hydrocarbon/NO_x runs it overpredicts the O_3 yield at the time of the first maximum.

Although the Paulson and Seinfeld mechanism [15] has some substantial differences from ours in terms of the O_3 + isoprene reactions, sensitivity calculations indicate that the main reason for the consistent underpredictions in reactivity is that the Paulson and Seinfeld mechanism has a 12% alkyl nitrate yield in the OH radical reaction [15], but only an 8% yield of radicals from the isoprene + $O(^3P)$ reaction. If that mechanism is modified to employ the lower y^{OH}_{RNO3} and higher y^{O}_{Rad} values used in our mechanism, much closer model simulation results are obtained [76].

DISCUSSION AND CONCLUSIONS

The atmospheric reactions of isoprene are complex, with a number of competing reaction routes occurring to non-negligible extents, and with a variety of highly reactive primary and secondary products being formed. Until recently, these complex reaction routes had so many uncertainties that any detailed isoprene mechanism would be largely speculation. However, laboratory studies have significantly improved our understanding of the isoprene photooxidation reactions in the last few years, and the development of a detailed isoprene mechanism with predictive capabilities has become feasible. For example, ~60% of the OH radical reaction products have been identified and quantified, and qualitative product information concerning the remaining routes is available. Improved data concerning the OH radical yield in the ozone reaction with isoprene has significantly reduced the uncertainties in this aspect of the mechanism. Essentially all of the OH radical reaction routes of isoprene's major products, methacrolein and methyl vinyl ketone, have been identified, and the recent measurement of the OH radical yields in their O_3 reactions provides important information on these reactions. Our improved understanding of the methacrolein and methyl vinyl ketone reaction systems leads, we believe, to significantly reduced uncertainties in our estimates of the atmospheric reactions of the other identified (but unquantified) major isoprene atmospheric oxidation products.

However, the isoprene mechanism is not without significant remaining uncertainties. *Quantitative* information is needed on the yields of the expected products of the OH radical reaction (besides methacrolein, methyl vinyl ketone, or formaldehyde). Precise measurement of the yields of alkyl nitrates in the OH radical reaction with isoprene would probably be the most important datum in terms of sensitivity of model simulations. Although the recent information on OH radical yields has addressed the most sensitive single uncertainty in the reactions of O_3 with isoprene and some of its products, the details of these reactions remain elusive. Other radicals are expected to be formed in the ozone reactions, with equal yields as the OH radical, but at present this aspect of the mechanism consists largely of speculation. The NO_3 + isoprene mechanism, which is important not only at nighttime but in affecting model performance in simulations of chamber experiments, has major uncertainties, the most important being the relative importance of radical formation *versus* NO_2 generation. Current laboratory studies of the NO_3 radical reaction with isoprene are not sufficiently representative of atmospheric conditions [24] to provide unambiguous information in this regard. Although the reaction of isoprene with $O(^3P)$ atoms is probably not important in the atmosphere, measurements of radical yields in this reaction would significantly improve the utility of environmental chamber data in evaluating or optimizing other aspects of the mechanism.

The subsequent reactions of the predicted but unquantified C_4- and C_5-unsaturated products is major source of uncertainty in the mechanism. These compounds are expected to be highly reactive, so measurements of their atmospherically-important rate constants are needed in addition to improved quantification of their yields. The extent to which these compounds react with OH radicals or O_3 under various conditions is presently uncertain. The consistent underprediction of PAN yields in isoprene-NO_x experiments, if not an experimental artifact, would most likely be due to model not representing these reactions correctly, since the model can predict PAN reasonably well in the experiments with methacrolein and MVK.

Finally, the quantum yields and mechanisms for photolyses of methacrolein and methyl vinyl ketone, isoprene's major photoreactive products, need to be determined with greater precision, and as a function of wavelength. Modeling the environmental chamber data indicate that the photodecompositions of methacrolein and methyl vinyl ketone, and probably the other unsaturated C_4- and C_5-carbonyl products, are non-negligible. Although there are some laboratory data concerning their quantum yields, these data have large uncertainties, the light sources employed is not a good representation of sunlight, and there is no information concerning wavelength dependences of the

quantum yields. Therefore, the quantum yields for atmospheric conditions could only be derived by adjusting them to fit model simulations of environmental chamber data. The possibility that this adjustment could be compensating for other errors in the methacrolein and MVK mechanisms cannot be ruled out.

Despite these uncertainties and the need to optimize some aspects of the mechanism to fit the chamber data, the results of the environmental chamber data evaluation are quite encouraging, and indicate that the mechanism may have reasonably good predictive capability, at least for formation of ozone, methacrolein, and methyl vinyl ketone from isoprene, and formation of ozone and PAN from methyl vinyl ketone and methacrolein. The set of environmental chamber data used to evaluate this mechanism is highly varied, consisting of outdoor as well as indoor chamber data, with the indoor runs employing two different types of light sources and two different types of reactor surfaces, and the outdoor runs being carried out at two different laboratories which generally employ significantly different operating procedures. Although the mechanism adjustments used only the indoor chamber data, the results of the simulations of the outdoor chamber runs were almost as satisfactory.

The one area where the performance of the mechanism was not satisfactory was the underprediction, by ~40%, of the yields of PAN in the isoprene experiments. However, the mechanism predicts that isoprene forms a variety of other PAN analogues as well as PAN itself, and the possibility of interferences in the GC analyses of PAN cannot be ruled out. More information is needed concerning PAN yields in the isoprene oxidation system using alternative measurement methods which are not subjective to the same interferences. If the discrepancy is real, it could be due either to errors in the other radicals, besides the OH radical, formed in the O_3 + isoprene reactions, or (more likely) errors in the assumed OH radical and/or O_3 reactions of the C_5-unsaturated carbonyl products. It may be related to an underprediction of methylglyoxal by this model, as hinted by the simulations of this product in a single outdoor chamber experiment (Figure 10), but obviously this has not been clearly established.

It should be recognized that although this mechanism is highly detailed in many respects, it uses a condensed and approximate method for representing the peroxy + peroxy and peroxy + HO_2 radical reactions which can become important at nighttime or in the absence of NO_x. Using a more detailed representation of these processes would significantly increase its size and complexity and, because of the uncertainties in the processes involved and the lack of chamber data suitable for

evaluating this aspect of the mechanism, may not necessarily improve its predictive capability. However, this mechanism can serve as the starting point for development of mechanisms which use a more detailed representation of these processes.

This mechanism is more detailed than needed for most airshed model applications, particularly those focused primarily on predictions of ozone formation. Its primary utility is therefore to serve as a starting point for the development of condensed mechanisms tailored to specific model applications. Most of the primary or secondary product species can be lumped together, or lumped with other species already in the standard mechanisms, without significantly affecting simulations of ozone and other species of interest. This approach would yield a more efficient mechanism if simulations of the specific product species is not of interest. The development of condensed versions of this mechanism, and comparison predictions of this mechanism with other condensed mechanisms currently used in airshed models, will is the subject of another paper [77].

ACKNOWLEDGEMENTS

The authors thank Dr. Harvey Jeffries and Dr. Ken Sexton of the University of North Carolina for making their environmental chamber data available for this work and for helpful discussions. We also thank Dr. Jeffries for providing a manuscript of their paper on the derivitization studies prior to publication, and Dr. Geert Moortgat of the Max-Planck-Institut für Chemie for providing us with a copy of his chapter on the photolyses of methacrolein and methyl vinyl ketone. The new SAPRC ETC, DTC, XTC, and OTC chamber experiments used in this work were carried out by John A. Pierce, Dogmin Luo, and Irina Malkina.

This work, and the new SAPRC chamber experiments, was funded primarily by the United States Environmental Protection Agency through Cooperative Agreement CR81773-01-3, with Dr. Marcia C. Dodge of EPA/AREAL as the EPA project officer. Roger Atkinson acknowledges partial support from the Agricultural Experiment Station, University of California, Riverside. William Carter acknowledges partial support from the California Air Resources Board through Contract No. 92-329. Although the research described in this article has been funded in part by these agencies, it has not been subjected to review by these agencies and therefore does not necessarily reflect the views of the agencies and no official endorsement should be inferred.

REFERENCES

[1] R. A. Rasmussen, *Environ. Sci. Technol.*, **4**, 667 (1970).
[2] R. A. Rasmussen, *J. Air. Pollut. Control Assoc*., **22**, 537 (1972).
[3] R. C. Evans, D. T. Tingey, M. L. Gumpertz, and W. F. Burns, *Bot. Gaz*., **143**, 304 (1982).
[4] V. A. Isidorov, I. G. Zenkevich, and B. V. Ioffe, *Atmos. Environ*., **19**, 1 (1985).
[5] A. B. Guenther, R. K. Monson, and R. Fall, *J. Geophys. Res*., **96**, 10799 (1991).
[6] B. Lamb, D. Gay, H. Westberg, and T. Pierce, *Atmos. Environ*., **27A**, 1673 (1993).
[7] M. Trainer, E. J. Willaims, D. D. Parrish, M. P. Buhr, E. J. Allwine, H. H. Westberg, F. C. Fehsenfeld, and S. C. Liu, *Nature*, **329**, 705 (1987).
[8] W. L. Chameides, R. W. Lindsay, J. Richardson, and C. S. Kiang, *Science*, **241**, 1473 (1988).
[9] S. Sillman, J. A. Logan, and S. C. Wofsy, *J. Geophys. Res*., **95**, 1837 (1990).
[10] A. C. Lloyd, R. Atkinson, F. W. Lurmann, and B. Nitta, *Atmos. Environ*., **17**, 1931 (1983).
[11] M. W. Gery, G. Z. Whitten, and J. P. Killus, "*Development and Testing of the CBM-IV For Urban and Regional Modeling*", EPA-600/3-88-012, January 1988.
[12] M. W. Gery, G. Z. Whitten, J. P. Killus, and M. C. Dodge, *J. Geophys. Res*., **94**, 12925 (1989).
[13] W. R. Stockwell, P. Middleton, J. S. Chang, and X. Tang, *J. Geophys. Res*., **95**, 16343 (1990).
[14] W. P. L. Carter, *Atmos. Environ*., **24A**, 481 (1990).
[15] S. E. Paulson and J. H. Seinfeld, *J. Geophys Res*., **97**, 20703 (1992).
[16] R. Atkinson, S. M. Aschmann, J. Arey, and B. Shorees, *J. Geophys. Res*., **97**, 6065 (1992).
[17] R. Atkinson, J. Arey, S. M. Aschmann, and E. C. Tuazon, *Res. Chem. Intermed*. **20**, 385 (1994).
[18] S. M. Aschmann and R. Atkinson, *Environ. Sci. Technol*., **28**, 1539 (1994).
[19] D. Pierotti, S. C. Wofsy, D. Jacob, and R. A. Rasmussen, *J. Geophys. Res*., **95**, 1871 (1990).
[20] R. S. Martin, H. Westberg, E. Allwine, L. Ashman, C. J. Farmer, and B. Lamb, *J. Atmos. Chem*., **13**, 1 (1991).
[21] S. A. Montzka, M. Trainer, P. D. Goldan, W. C. Kuster, and F. C. Fehsenfeld, *J. Geophys. Res*., **98**, 1101 (1993).
[22] Y. Yokouchi, *Atmos. Environ*., **28**, 2651 (1994).
[23] S. A. Montzka, M. Trainer, W. M. Angevine, and F. C. Fehsenfeld, *J. Geophys. Res*., **100**, 11393 (1995).
[24] R. Atkinson, *J. Phys. Chem. Ref. Data*, **Monograph 2**, 1 (1994).
[25] R. Atkinson, *J. Phys. Chem. Ref. Data*, **Monograph 1**, 1 (1989).
[26] R. Atkinson, *J. Phys. Chem. Ref. Data*, **20**, 459 (1991).
[27] S. E. Paulson, R. C. Flagan, and J. H. Seinfeld, *Int. J. Chem. Kinet*., **24**, 79 (1992).
[28] S. E. Paulson, J. J. Orlando, G. S. Tyndall, and J. G. Calvert, *Int. J. Chem. Kinet*., **27**, 997 (1995).
[29] R. Atkinson, S. M. Aschmann, E. C. Tuazon, J. Arey, and B. Zielinska, *Int. J. Chem. Kinet*., **21**, 593 (1989).
[30] E. C. Tuazon and R. Atkinson, *Int. J. Chem. Kinet*., **22**, 1221 (1990).
[31] A. Miyoshi, S. Hatakeyama, and N. Washida, *J. Geophys. Res*., **99**, 18799 (1994).
[32] E. S. C. Kwok, R. Atkinson, and J. Arey, *Environ. Sci. Techmol*., **29**, 2467 (1995).
[33] J. Yu, H. E. Jeffries, and R. M. Le Lacheur, *Environ. Sci. Technol*., **29**, 1923 (1995).
[34] S. E. Paulson, R. C. Flagan, and J. H. Seinfeld, *Int. J. Chem. Kinet*., **24**, 103 (1992).
[35] H. Skov, J. Hjorth, C. Lohse, N. R. Jensen, and G. Restelli, *Atmos. Environ*., **26A**, 2771 (1992).

[36] E. S. C. Kwok, S. M. Aschmann, J. Arey, and R. Atkinson, *Int. J. Chem. Kinet*., to be submitted for publication (1996).
[37] E. C. Tuazon and R. Atkinson, *Int. J. Chem. Kinet*., **21**, 1141 (1989).
[38] E. C. Tuazon and R. Atkinson, *Int. J. Chem Kinet*., **22**, 591 (1990).
[39] W. P. L. Carter, D. Luo, I. L. Malkina, and D. Fitz, "*The University of California, Riverside Environmental Chamber Data Base for Evaluating Oxidant Mechanism. Indoor Chamber Experiments through 1993*", Report submitted to the U.S. Environmental Protection Agency, EPA/AREAL, Research Triangle Park, NC., March 20, 1995. (This report and data base are available on the Internet by anonymous FTP at cert.ucr.edu, directories pub/carter/pubs and pub/carter/chdata.)
[40] W. P. L. Carter and F. W. Lurmann, *"Evaluation of the RADM Gas-Phase Chemical Mechanism"*, Final Report, EPA-600/3-90-001 (1990).
[41] W. P. L. Carter and F. W. Lurmann, *Atmos. Environ.* **25A**, 2771 (1991).
[42] W. P. L. Carter, *Atmos. Environ*., **29**, 2513 (1995).
[43] W. P. L. Carter, D. Luo, I. L. Malkina, and J. A. Pierce, "*An Experimental and Modeling Study of the Photochemical Ozone Reactivity of Acetone*," Final Report to Chemical Manufacturers Association Contract No. KET-ACE-CRC-2.0. December 10, 1993. (This report is available on the Internet by anonymous FTP at cert.ucr.edu, directory pub/carter/pubs.)
[44] D. Grosjean, E. L. Williams II, and E. Grosjean, *Environ. Sci. Technol*., **27**, 830 (1993).
[45] S. M. Aschmann, J. Arey, and R. Atkinson, *Atmos. Environ*., in press (1996).
[46] E. P. Gardner, P. D. Sperry, and J. G. Calvert, *J. Phys. Chem*., **91**, 1922 (1987).
[47] W. H. Raber and G. K. Moortgat, "Photooxidation of Selected Carbonyl Compounds in Air: Methyl Ethyl Ketone, Methyl Vinyl Ketone, Methacrolein, and Methylglyoxal," in "Progress and Problems in Atmospheric Chemistry", John Barker, ed., World Scientific Publishing, pp 319-373, in press.
[48] R. Atkinson, D. L. Baulch, R. A. Cox, R. F. Hampson, Jr., J. A. Kerr, M. J. Rossi, and J. Troe, *J. Phys. Chem. Ref. Data*, submitted for publication (1995).
[49] J. D. Rogers, *J. Phys. Chem*., **94**, 4011 (1990).
[50] C. A. Cantrell, J. A. Davidson, A. H. McDaniel, R. E. Shetter, and J. G. Calvert, *J. Phys. Chem*., **94**, 3902 (1990).
[51] E. S. C. Kwok and R. Atkinson, *Atmos. Environ*., **29**, 1685 (1995).
[52] R. Atkinson, *Int. J. Chem. Kinet*., **19**, 799 (1987).
[53] W. P. L. Carter, A. M. Winer, R. Atkinson, M. C. Dodd, and S. M. Aschmann, *"Atmospheric Photochemical Modeling of Turbine Engine Fuels. Phase I. Experimental studies. Volume I of II. Results and Discussion."* Final Report to the U. S. Air Force, ESL-TR-84-32, September (1994).
[54] A. Alvarado, R. Atkinson, and J. Arey, *Int. J. Chem. Kinet*., to be submitted for publication.
[55] H. Niki, P. D. Maker, C. M. Savage, and M. D. Hurley, *J. Phys. Chem*., **91**, 2174 (1987).
[56] P. Dagaut, R. Liu, T. J. Wallington, and M. J. Kurylo, *J. Phys. Chem*., **93**, 7378 (1989).
[57] C. N. Plum, E. Sanhueza, R. Atkinson, W. P. L. Carter, and J. N. Pitts, Jr., *Environ. Sci. Technol*., **17**, 479 (1983).
[58] I. R. Slagle, J.-Y Park, M. C. Heaven, and D. Gutman, *J. Am. Chem. Soc*., **106**, 4356 (1984).
[59] J. M. Roberts and S. B. Bertman, *Int. J. Chem. Kinet*., **24**, 297 (1992).
[60] W. P. L. Carter and R. Atkinson, *J. Atmos. Chem*., **8**, 165 (1989).
[61] R. J. Cvetanovic, *Can. J. Chem*., **36**, 623 (1958).
[62] R. J. Cvetanovic and L. C. Doyle, *Can. J. Chem*., **38**, 2187 (1960).
[63] R. J. Cvetanovic, *Adv. Photochem*., **1**, 115 (1963).

[64] J. N. Pitts, Jr., K. Darnall, W. P. L. Carter, A. M. Winer, and R. Atkinson, *Mechanisms of Phochemical Reactions in Urban Air*", EPA-600/3-79-110, U. S. Evironmental Protection Agency, Environmental Research Laboratory, Research Triangle Park, NC, November 1979.

[65] W. P. L. Carter, D. Luo, I. L. Malkina, and J. A. Pierce, "*Environmental Chamber Studies of Atmospheric Reactivities of Volatile Organic Compounds. Effects of Varying Chamber and Light Source*", Final report to National Renewable Energy Laboratory, Contract XZ-2-12075, Coordinating Research Council, Inc., Project M-9, California Air Resources Board, Contract A032-0692, and South Coast Air Quality Management District, Contract C91323, March 26, 1995. (This report is available on the Internet by anonymous FTP at cert.ucr.edu, directory pub/carter/pubs.)

[66] H. E. Jeffries, R. M. Kamens, K. G. Sexton, and A. A. Gerhardt, "*Outdoor Smog Chamber Experiments to Test Photochemical Models*", EPA-600/3-82-016a, April, 1982.

[67] H. E. Jeffries, K. G. Sexton, R. M. Kamens, and M. S. Holleman, "*Outdoor Smog Chamber Experiments to Test Photochemical Models: Phase II*", Final Report, EPA-600/3-85-029, 1985.

[68] F. Liu, "Development and Application of an Analytical Method for Measurements of Hydroxy acetone and glycoaldehyde in Air", Masters Thesis, Dept ESE, University of North Carolina-Chapel Hill, 1992.

[69] Y.-H. Li, "DNPH Derivatives for Measurement of Hydroxycarbonyls in the Oxidation Products of Isoprene," Masters Thesis, Dept. ESE, University of North Carolina-Chapel Hill, 1994.

[70] H. E. Jeffries, M. W. Gery, and W. P. L. Carter, "*Protocol for Evaluating Oxidant Mechanisms for Urban and Regional Models*", Report for U. S. Environmental Protection Agency Cooperative Agreement No. 815779, Atmospheric Research and Exposure Assessment Laboratory, Research Triangle Park, NC, 1992.

[71] H. E. Jeffries, K. G. Sexton, J. R. Arnold, and T. L. Kale, "*Validation Testing of New Mechanisms with Outdoor Chamber Data. Volume 3: Calculation of Photochemical Reaction Photolysis Rates in the UNC Outdoor Chamber*", Final Report, EPA-600/3-89-010c, 1989.

[72] W. P. L. Carter, R. Atkinson, A. M. Winer, and J. N. Pitts, Jr., *Int. J. Chem. Kinet.*, **14**, 1071 (1982).

[73] W. P. L. Carter, J. A. Pierce, D. Luo, and I. L. Malkina, *Atmos. Environ.*, **29**, 2499 (1995).

[74] G. M. Johnson, "*Factors Affecting Oxidant Formation in Sydney Air," in "The Urban Atmosphere -- Sydney, a Case Study*", Eds., J. N. Carras and G. M. Johnson (CSIRO, Melbourne), pp. 393-408, 1983.

[75] W. P. L. Carter and R. Atkinson, *Environ. Sci. Technol.*, **21**, 670 (1987).

[76] W. P. L. Carter, D. Luo, I. L. Malkina, and J. A. Pierce, "*Evaluation of Chemical Mechanisms for Atmospheric Ozone Formation from Biogenic Compounds*", presented at the A&WMA International Conference on Regional Photochemical Measurementa and Modeling Studies, San Diego, CA, November 8-12, 1993.

[77] W. P. L. Carter, *Atmos. Environ.*, submitted for publication (1995).

Table 1. Listing of the detailed mechanism for the NO_x - air reactions of isoprene and its products. [a]

Kinetic Parameters [b]				Notes	Reactions
k(300)	A	Ea	B	[c]	
Isoprene					
9.97E-11	2.54E-11	-0.81	0.00	1,2	ISOP + HO. = 0.088 RO2-N. + 0.912 RO2-R. + 0.629 HCHO + 0.23 METHACRO + 0.32 MVK + 0.079 HOMACR + 0.159 IP-MHY + 0.079 IP-HMY + 0.045 MEFURAN + 0.079 R2O2. + #1.079 RO2.
1.34E-17	7.86E-15	3.80	0.00	1,3	Isoprene + O3 = 0.4 HCHO + 0.39 METHACRO + 0.16 MVK + 0.55 (HCHO2) + 0.2 (C:CC(C)O2) + 0.2 (C:C(C)CHO2) + 0.05 ISO-OX
	(fast)			4	(HCHO2) = 0.12 {HO2. + CO + HO.} + 0.18 {H2 + CO2} + 0.7 HCOOH
	(fast)			3	(C:CC(C)O2) = HO. + R2O2. + HCHO + AC-RCO3. + RO2. + RCO3.
	(fast)			3,5	(C:C(C)CHO2) = 0.75 {RCHO + -C} + 0.25 {PROPENE + CO2}
3.60E-11	(No T Dependence)			6	Isoprene + O = 0.75 ISO-OX + 0.25 {AC-RCO3. + RCO3. + 2 HCHO + RO2-R. + RO2.}
6.85E-13	3.03E-12	0.89	0.00	1,7	Isoprene + NO3 = 0.8 {RCHO-NO3 + RO2-R.} + 0.2 {IP-MHY + R2O2. + NO2} + RO2.
1.50E-19	(No T Dependence)			8,9	Isoprene + NO2 = 0.8 {RCHO-NO3 + RO2-R.} + 0.2 {IP-MHY + R2O2. + NO} + RO2.
Primary Isoprene Products					
Methacrolein					
3.33E-11	1.86E-11	-0.35	0.00	10,11	METHACRO + HO. = 0.5 {MA-RCO3. + RCO3.} + 0.42 {HOACET + CO} + 0.08 {HCHO + MGLY} + 0.5 {RO2-R. + RO2.}
1.19E-18	1.36E-15	4.20	0.00	1,12	METHACRO + O3 = 0.9 {(HCHO2) + MGLY} + 0.1 {HCHO + (C2(O2)CHO)}
	(fast)			13	(C2(O2)CHO) = HO. + R2O2. + HCHO + HCOCO-O2. + RO2. + RCO3.
(Abs. Coefs = ACROLEIN)				14,15	METHACRO + HV = 0.66 HO2. + 0.33 MA-RCO3. + 0.67 {CO + HCHO + CCO-O2.} + 0.34 {HO. + R2O2. + RO2.} + RCO3.
(Overall Q.Y. = 0.0036)					
4.75E-15	1.50E-12	3.43	0.00	16	METHACRO + NO3 = 0.5 {MA-RCO3. + RCO3. + HNO3} + 0.5 {CO + HO2. + RNO3 + -2 -C + R2O2. + RO2.}
Methyl Vinyl Ketone					
1.87E-11	4.14E-12	-0.90	0.00	10,17	MVK + HO. = 0.7 {HOCCHO + R2O2. + CCO-O2. + RCO3.} + 0.3 {HCHO + MGLY + RO2-R.} + RO2.
4.74E-18	7.51E-16	3.02	0.00	1,12	MVK + O3 = 0.95 {(HCHO2) + MGLY} + 0.05 {HCHO + (C-CO-CHO2)}
	(fast)			18	(C-CO-CHO2) = (C2(O2)CHO)
(Abs. Coefs = ACRROLEIN)				14,19	MVK + HV = 0.7 {PROPENE + CO} + 0.3 {HCHO + RO2-R. + AC-RCO3. + RCO3.}
(Overall Q.Y. = 0.0111)					
	(slow)			20	MVK + NO3 = products
Formaldehyde					
9.76E-12	1.13E-12	-1.29	2.00		HCHO + HO. = HO2. + CO + H2O
(Phot. Set = HCHONEWR)				21	HCHO + HV = 2 HO2. + CO
(Phot. Set = HCHONEWM)				21	HCHO + HV = H2 + CO
7.79E-14	9.70E-15	-1.24	0.00		HCHO + HO2. = HOCOO.
1.77E+02	2.40E+12	13.91	0.00		HOCOO. = HO2. + HCHO
(Same k as for RO2.)					HOCOO. + NO = -C + NO2 + HO2.
6.38E-16	2.80E-12	5.00	0.00		HCHO + NO3 = HNO3 + HO2. + CO
Hydroxymethacrolein					
4.3E-11	(No T Dependence)			22	HOMACR + HO. = 0.38 {HOMA-RCO3. + RCO3.} + 0.52 {HOACET + CO} + 0.10 {HCHO + MGLY} + 0.62 {RO2-R. + RO2.}
(Same k as for METHACRO)				22	HOMACR + O3 = 0.9 {(HCHO2) + MGLY} + 0.1 {HCHO + (HOC2(O2)CHO)}
	(fast)				(HOC2(O2)CHO) = HO. + CO + GLY + HO2.
(Same k as for METHACRO)				22	HOMACR + HV = HO2. + CO + HCHO + HOCCO-O2. + RCO3.
(Same k as for METHACRO)				22	HOMACR + NO3 = 0.5 {HOMA-RCO3. + RCO3. + HNO3} + 0.5 {CO + HO2. + RNO3 + -2 -C + R2O2. + RO2.}
$HOCH_2CH=C(CH_3)CHO$					
7.00E-11	(No T Dependence)			23,24	IP-MHY + HO. = 0.25 {MHY-RCO3. + RCO3.} + 0.50 {MEK + CO} + 0.25 {HOCCHO + MGLY} + 0.75 {RO2-R. + RO2.}
1.00E-17	(No T Dependence)			25,26	IP-MHY + O3 = 0.9 {MGLY + (HOCCHO2)} + 0.1 {HOCCHO + (C2(O2)CHO)}
	(fast)			27	(HOCCHO2) = 0.6 HO. + 0.3 {HOCCO-O2. + RCO3.} + 0.3 {RO2-R. + HCHO + CO + RO2.} + 0.8 -C
(Same k as for METHACRO)				22	IP-MHY + HV = CO + HO2. + HOCCHO + CCO-O2. + RCO3.
1.00E-13	(No T Dependence)			28,29	IP-MHY + NO3 = RNO3 + -1 -C + CO + HO2. + R2O2. + RO2.

Table 1 (continued)

Kinetic Parameters [a]				Notes	Reactions
k(300)	A	Ea	B	[b]	
$HOCH_2C(CH_3)$=CHCHO					
(Same k as for IP-MHY)				23,24	IP-HMY + HO. = 0.25 {HMY-RCO3. + RCO3.} + 0.50 {GLY + HOACET} + 0.25 {RCHO + -C + CO} + 0.75 {RO2-R. + RO2.}
(Same k as for IP-MHY)				25,26	IP-HMY + O3 = 0.9 {HOACET + (HCOCHO2)} + 0.1 {GLY + (C2(O2)COH)}
(fast)				30	(HCOCHO2) = 0.12 {HO2. + 2 CO + HO.} + 0.74 -C + 0.51 {CO2 + HCHO}
(fast)				31	(C2(O2)COH) = HO. + MGLY + HO2. + R2O2. + RO2.
(Same k as for METHACRO)				22	IP-HMY + HV = CO + HO2. + HOACET + CO + HO2.
(Same k as for IP-MHY)				28,29	IP-HMY + NO3 = RCHO-NO3 + -1 -C + HCHO + HO2. + R2O2. + RO2.
3-Methylfuran					
9.35E-11	(No T Dependence)			10,32	HO. + MEFURAN = 0.245 {R2O2. + RO2.} + HO2. + 0.475 HET-UNKN + 4.05 -C
(Abs. Coefs = ACROLEIN)				32	HET-UNKN + HV = HO2. + CCO-O2. + RCO3.
(Overall Q.Y. = 1)					
2.05e-17	(No T Dependence)			33	O3 + MEFURAN = 0.6 {HO. + AC-RCO3. + R2O2. + RO2. + RCO3.} + 0.4 RCHO + 2 -C
1.31E-11	(No T Dependence)			34	NO3 + MEFURAN = 0.245 {R2O2. + RO2.} + NO2 + 0.475 HET-UNKN + 4.05 -C
Isoprene Epoxides (Represented by 1,2-Epoxy-2-methyl-3-butene)					
3.11E-11	6.55E-12	-0.93	0.00	35	ISO-OX + HO. = HCHO + 0.75 {HOCCHO + CCO-O2. + RCO3.} + 0.25 {HOACET + HO2. + CO}
(slow)				36	ISO-OX + O3 = products
Lumped C_5 Nitrato Aldehyde Products					
2.00E-11	(No T Dependence)			37	RCHO-NO3 + HO. = NA-RCO3. + RCO3.
(Phot. Set = CCHOR)				37	RCHO-NO3 + HV = 2 {CO + HO2.} + RNO3 + -2 -C
2.84E-15	1.40E-12	3.70	0.00	37	RCHO-NO3 + NO3 = HNO3 + NA-RCO3. + RCO3.
Propene (minor product in O_3 + isoprene reaction)					
2.60E-11	4.85E-12	-1.00	0.00		PROPENE + HO. = RO2-R. + RO2. + HCHO + CCHO
1.05E-17	5.51E-15	3.73	0.00	6	PROPENE + O3 = 0.6 HCHO + 0.4 CCHO + 0.4 (HCHO2) + 0.6 (CCHO2)
(fast)				38	(CCHO2) = 0.25 CCOOH + 0.15 {CH4 + CO2} + 0.6 HO. + 0.3 {CCO-O2. + RCO3.} + 0.3 {RO2-R. + HCHO + CO + RO2.}
9.73E-15	4.59E-13	2.30	0.00	39	PROPENE + NO3 = R2O2. + RO2. + HCHO + CCHO + NO2
4.01E-12	1.18E-11	0.64	0.00		PROPENE + O = 0.4 HO2. + 0.5 RCHO + 0.5 MEK + -0.5 -C
Secondary Isoprene Products					
Glycoaldehyde					
9.90E-12	(No T Dependence)			40	HOCCHO + HO. = 0.8 {HOCCO-O2. + H2O + RCO3.} + 0.2 {GLY + HO2.}
(Phot. Set = CCHOR)				37	HOCCHO + HV = CO + HCHO + 2 HO2.
2.84E-15	1.40E-12	3.70	0.00	37	HOCCHO + NO3 = HNO3 + HOCCO-O2. + RCO3.
Hydroxyacetone					
3.00E-12	(No T Dependence)			41	HOACET + HO. = MGLY + HO2.
(Phot. Set = ACET-93C)				42	HOACET + HV = CCO-O2. + RCO3. + HCHO + HO2.
Methylglyoxal					
1.72E-11	(No T Dependence)				MGLY + HO. = CO + CCO-O2. + RCO3.
(Phot. Set = MEGLYOX1)				43	MGLY + HV = HO2. + CO + CCO-O2. + RCO3.
(Abs. Coefs = MEGLYOX2)				43	MGLY + HV = HO2. + CO + CCO-O2. + RCO3.
(Overall Q.Y. = 0.107)					
(Same k as for RCHO)					MGLY + NO3 = HNO3 + CO + CCO-O2. + RCO3.
Glyoxal					
1.14E-11	(No T Dependence)				GLY + HO. = 0.6 HO2. + 1.2 CO + 0.4 {HCOCO-O2. + RCO3.}
(Phot. Set = GLYOXAL1)				43	GLY + HV = 0.8 HO2. + 0.45 HCHO + 1.55 CO
(Abs. Coefs = GLYOXAL2)				43	GLY + HV = 0.13 HCHO + 1.87 CO
(Overall Q.Y. = 0.029)					
(Same k as for RCHO)					GLY + NO3 = HNO3 + 0.6 HO2. + 1.2 CO + 0.4 {HCOCO-O2. + RCO3.}

Table 1 (continued)

Kinetic Parameters [a]				Notes	Reactions
k(300)	A	Ea	B	[b]	
					General Lumped Product Species
					Lumped Higher Aldehyde (Propionaldehyde)
1.97E-11	8.50E-12	-0.50	0.00		RCHO + HO. = C2CO-O2. + RCO3.
(Phot. Set = RCHO)					RCHO + HV = CCHO + RO2-R. + RO2. + CO + HO2.
2.84E-15	1.40E-12	3.70	0.00		NO3 + RCHO = HNO3 + C2CO-O2. + RCO3.
					Lumped Higher Ketone or Other Non-Aldehyde Oxygenated Product (Methylethyl ketone)
1.16E-12	2.92E-13	-0.82	2.00		MEK + HO. = H2O + 0.5 {CCHO + HCHO + CCO-O2. + C2CO-O2.} + RCO3. + 1.5 {R2O2. + RO2.}
(Abs. Coefs = KETONE)					MEK + HV = CCO-O2. + CCHO + RO2-R. + RCO3. + RO2.
(Overall Q.Y = 0.1)					
					Lumped Non-Aldehyde Organic Nitrate
2.07E-12	2.19E-11	1.41	0.00		RNO3 + HO. = NO2 + 0.155 MEK + 1.05 RCHO + 0.48 CCHO + 0.16 HCHO + 0.11 -C + 1.39 {R2O2. + RO2.}
					Lumped Hydroperoxide Group [d]
(Phot. Set = CO2H)					-OOH + HV = HO2. + HO.
1.81E-12	1.18E-12	-0.25	0.00		HO. + -OOH = HO.
3.71E-12	1.79E-12	-0.44	0.00		HO. + -OOH = RO2-R. + RO2.
					Peroxy Radical Operators [e]
					Total Peroxy Radical Counter (for determining rates of RO_2 + RO_2 reactions) [f]
7.68E-12	4.20E-12	-0.36	0.00		RO2. + NO = NO
4.90E-12	3.40E-13	-1.59	0.00		RO2. + HO2. = HO2.
1.00E-15	(No T Dependence)				RO2. + RO2. =
1.09E-11	1.86E-12	-1.05	0.00		RO2. + RCO3. =
					Total Acylperoxy Radical Counter (for determining rates of RCO_3 + RO_2 and RCO_3 + RCO_3 reactions) [f]
2.25E-11	(Falloff Kinetics)			44	RCO3. + NO = NO
k0 =	5.65E-28	0.00	-7.10		
kINF =	2.64E-11	0.00	-0.90		
F= 0.27					
1.04E-11	(Falloff Kinetics)			44	RCO3. + NO2 = NO2
k0 =	2.57E-28	0.00	-7.10		
kINF =	1.20E-11	0.00	-0.90		
F= 0.30					
4.90E-12	3.40E-13	-1.59	0.00		RCO3. + HO2. = HO2.
1.64E-11	2.80E-12	-1.05	0.00		RCO3. + RCO3. =
					Peroxy Radical Operator for Overall Effect of one NO to NO_2 Conversion and Formation of HO_2
(Same k as for RO2.)					RO2-R. + NO = NO2 + HO2.
(Same k as for RO2.)					RO2-R. + HO2. = -OOH [d]
(Same k as for RO2.)					RO2-R. + RO2. = RO2. + 0.5 HO2. [e,f]
(Same k as for RO2.)					RO2-R. + RCO3. = RCO3. + 0.5 HO2. [e,f]
					Peroxy Radical Operator for Overall Effect of Alkyl Nitrate Formation from Reactions of RO_2 + NO
(Same k as for RO2.)					RO2-N. + NO = RNO3
(Same k as for RO2.)					RO2-N. + HO2. = -OOH + MEK + 1.5 -C
(Same k as for RO2.)					RO2-N. + RO2. = RO2. + 0.5 HO2. + MEK + 1.5 -C
(Same k as for RO2.)					RO2-N. + RCO3. = RCO3. + 0.5 HO2. + MEK + 1.5 -C
					Peroxy Radical Operator Effect of an Additional NO to NO_2 Conversion in Multi-Step Mechanisms
(Same k as for RO2.)					R2O2. + NO = NO2
(Same k as for RO2.)					R2O2. + HO2. =
(Same k as for RO2.)					R2O2. + RO2. = RO2.
(Same k as for RO2.)					R2O2. + RCO3. = RCO3.

Table 1 (continued)

Kinetic Parameters [a]				Notes	Reactions
k(300)	A	Ea	B	[b]	
					Individual Acyl Peroxy Radicals, PAN and PAN Analogues [e]
					Acetyl Peroxy Radicals and PAN
	(Same k as for RCO3.)				CCO-O2. + NO = CO2 + NO2 + HCHO + RO2-R. + RO2.
	(Same k as for RCO3.)				CCO-O2. + NO2 = PAN
	(Same k as for RCO3.)				CCO-O2. + HO2. = -OOH + CO2 + HCHO
	(Same k as for RCO3.)				CCO-O2. + RO2. = RO2. + 0.5 HO2. + CO2 + HCHO
	(Same k as for RCO3.)				CCO-O2. + RCO3. = RCO3. + HO2. + CO2 + HCHO
6.50E-04	(Falloff Kinetics)			44	PAN = CCO-O2. + NO2 + RCO3.
k0 =	4.90E-03	23.97	0.00		
kINF =	4.00E+16	27.08	0.00		
	F= 0.30				
	CH_2=C(CH_3)CO-OO· and CH_2=C(CH_3)CO-OONO_2				
	(Same k as for RCO3.)			45	MA-RCO3. + NO = NO2 + CO2 + HCHO + CCO-O2. + RCO3.
	(Same k as for C2CO-O2.)				MA-RCO3. + NO2 = MA-PAN
	(Same k as for RCO3.)				MA-RCO3. + HO2. = -OOH + 2 {HCHO + CO2}
	(Same k as for RCO3.)				MA-RCO3. + RO2. = RO2. + 0.5 HO2. + 2 {HCHO + CO2}
	(Same k as for RCO3.)				MA-RCO3. + RCO3. = RCO3. + HO2. + 2 {HCHO + CO2}
4.79E-04	1.60E+16	26.80	0.00	46	MA-PAN = MA-RCO3. + NO2 + RCO3.
	H_2C=CHCO-OO· and H_2C=CHCO-OONO_2				
	(Same k as for RCO3.)			47	AC-RCO3. + NO = NO2 + CO2 + HCHO + CO + HO2.
	(Same k as for C2CO-O2.)				AC-RCO3. + NO2 = AC-PAN
	(Same k as for RCO3.)				AC-RCO3. + HO2. = -OOH + HCHO + CO + CO2
	(Same k as for RCO3.)				AC-RCO3. + RO2. = RO2. + 0.5 HO2. + HCHO + CO + CO2
	(Same k as for RCO3.)				AC-RCO3. + RCO3. = RCO3. + HO2. + HCHO + CO + CO2
	(Same k as for MA-PAN)				AC-PAN = AC-RCO3. + NO2 + RCO3.
	CH_2=C(CH_2OH)CO-OO· and CH_2C(CH_2OH)CO-OONO_2				
	(Same k as for RCO3.)			48	HOMA-RCO3. + NO = NO2 + CO2 + HCHO + HOCCO-O2. + RCO3.
	(Same k as for C2CO-O2.)				HOMA-RCO3. + NO2 = HOMA-PAN
	(Same k as for RCO3.)				HOMA-RCO3. + HO2. = -OOH + 2 {HCHO + CO2}
	(Same k as for RCO3.)				HOMA-RCO3. + RO2. = RO2. + 0.5 HO2. + 2 {HCHO + CO2}
	(Same k as for RCO3.)				HOMA-RCO3. + RCO3. = RCO3. + HO2. + 2 {HCHO + CO2}
	(Same k as for MA-PAN)				HOMA-PAN = MA-RCO3. + NO2 + RCO3.
	$HOCH_2CH$=C(CH_3)CO-OO· and $HOCH_2CH$=C(CH_3)CO-OONO_2				
	(Same k as for RCO3.)			48	MHY-RCO3. + NO = NO2 + CO2 + HOCCHO + CCO-O2. + RCO3.
	(Same k as for C2CO-O2.)				MHY-RCO3. + NO2 = MHY-PAN
	(Same k as for RCO3.)				MHY-RCO3. + HO2. = -OOH + 2 CO2 + HCHO + HOCCHO
	(Same k as for RCO3.)				MHY-RCO3. + RO2. = RO2. + 0.5 HO2. + 2 CO2 + HCHO + HOCCHO
	(Same k as for RCO3.)				MHY-RCO3. + RCO3. = RCO3. + HO2. + 2 CO2 + HCHO + HOCCHO
	(Same k as for MA-PAN)				MHY-PAN = MHY-RCO3. + NO2 + RCO3.
	$HOCH_2C(CH_3)$=CHCO-OO· and $HOCH_2C(CH_3)$=CHCO-OONO_2				
	(Same k as for RCO3.)			49	HMY-RCO3. + NO = NO2 + CO2 + HOACET + CO + HO2.
	(Same k as for C2CO-O2.)				HMY-RCO3. + NO2 = HMY-PAN
	(Same k as for RCO3.)				HMY-RCO3. + HO2. = -OOH + CO2 + CO + HOACET
	(Same k as for RCO3.)				HMY-RCO3. + RO2. = RO2. + 0.5 HO2. + CO2 + CO + HOACET
	(Same k as for RCO3.)				HMY-RCO3. + RCO3. = RCO3. + HO2. + CO2 + CO + HOACET
	(Same k as for MA-PAN)				HMY-PAN = HMY-RCO3. + NO2 + RCO3.
	$HOCH_2$CO-OO· and $HOCH_2$CO-OONO_2				
	(Same k as for RCO3.)				HOCCO-O2. + NO = CO2 + NO2 + HCHO + HO2.
	(Same k as for RCO3.)				HOCCO-O2. + NO2 = HO-PAN
	(Same k as for RCO3.)				HOCCO-O2. + HO2. = -OOH + CO2 + HCHO
	(Same k as for RCO3.)				HOCCO-O2. + RO2. = RO2. + 0.5 HO2. + CO2 + HCHO
	(Same k as for RCO3.)				HOCCO-O2. + RCO3. = RCO3. + HO2. + CO2 + HCHO
	(Same k as for RCO3.)				HO-PAN = HOCCO-O2. + NO2 + RCO3.
	HCOCO-OO· and HCOCO-OONO_2				
	(Same k as for RCO3.)				HCOCO-O2. + NO = NO2 + CO2 + CO + HO2.
	(Same k as for RCO3.)				HCOCO-O2. + NO2 = GPAN
	(Same k as for RCO3.)				HCOCO-O2. + HO2. = -OOH + CO2 + CO
	(Same k as for RCO3.)				HCOCO-O2. + RO2. = RO2. + 0.5 HO2. + CO2 + CO
	(Same k as for RCO3.)				HCOCO-O2. + RCO3. = RCO3. + HO2. + CO2 + CO
	(Same k as for PAN)				GPAN = HCOCO-O2. + NO2 + RCO3.

Table 1 (continued)

Kinetic Parameters [a]				Notes	Reactions
k(300)	A	Ea	B	[b]	
					Acylperoxy Radicals and PAN Analogue from Lumped Higher Aldehyde ($CH_3CH_2CO\text{-}OO\cdot$ and PPN)
(Same k as for RCO3.)					C2CO-O2. + NO = CCHO + RO2-R. + CO2 + NO2 + RO2.
8.40E-12	(No T Dependence)				C2CO-O2. + NO2 = PPN
(Same k as for RCO3.)					C2CO-O2. + HO2. = -OOH + CCHO + CO2
(Same k as for RCO3.)					C2CO-O2. + RO2. = RO2. + 0.5 HO2. + CCHO + CO2
(Same k as for RCO3.)					C2CO-O2. + RCO3. = RCO3. + HO2. + CCHO + CO2
6.78E-04	1.60E+17	27.97	0.00		PPN = C2CO-O2. + NO2 + RCO3.
					Acylperoxy Radical and PAN Analogue from Lumped Nitrato Aldehydes
(Same k as for RCO3.)				50	NA-RCO3. + NO = NO2 + CO2 + CO + HO2. + RNO3 + -2 -C
(Same k as for C2CO-O2.)					NA-RCO3. + NO2 = NA-PAN
(Same k as for RCO3.)					NA-RCO3. + HO2. = -OOH + CO2 + CO + RNO3 + -2 -C
(Same k as for RCO3.)					NA-RCO3. + RO2. = RO2. + 0.5 HO2. + CO2 + CO + RNO3 + -2 -C
(Same k as for RCO3.)					NA-RCO3. + RCO3. = RCO3. + HO2. + CO2 + CO + RNO3 + -2 -C
(Same k as for PPN)					NA-PAN = NA-RCO3. + NO2 + RCO3.

[a] This listing is available on the Internet by anonymous FTP at cert.ucr.edu, directory /pub/carter/mech.

[b] Except as noted, the expression for rate constant is $k = A\ e^{Ea/RT}\ (T/300)^B$. Rate constants and A factor are in ppm, min units. Units of Ea is kcal $mole^{-1}$. "Phot Set" or "Abs. Coefs" means this is a photolysis reaction, with the absorption coefficients and (for "Phot Set") quantum yields given by Carter [14] or in the reference cited. "Overall Q.Y." means that the rate constant for this photolysis reaction is calculated using the indicated absorption cross section data, together with the wavelength-independent quantum yield indicated. "Falloff kinetics" means that the rate constant is given by $k(M,T) = [k_0 M/(1+k_0 M/k_\infty)]\cdot F^X$, where $X=\{1+[\log_{10}(k_0 M/k_\infty)]^2\}^{-1}$, and k_0, k_∞, and F are given in the listing. If a rate constant is given as "(fast)", then the steady state approximation can be employed on the reacting species, and any arbitrary rate constant can be used. Alternatively, the species could be replaced in reactions forming it with the set of products formed in the "fast" reaction.

[c] Documentation notes are as follows. If no documentation notes are given, then the mechanism is the same as that given by Carter [14].

1 Rate constant expression recommended by Atkinson [24].

2 See discussion in text and Figure 1. HOMACR is $H_2C=C(CH_2OH)CHO$ (hydroxymethacrolein); IP-HMY is $HOCH_2C(CH_3)=CHCHO$; and IP-MHY is $HOCH_2CH=C(CH_3)CHO$. Assuming alkyl nitrate formation occurs 8.8% of the time gives best fits of model simulations to results of the isoprene - NO_x chamber experiments if it is assumed that the radical yield in the $O(^3P)$ + isoprene is 25.% (see text). The various other possible reaction pathways are shown on Figure 1. Pathways F, J, and K+L are assumed to occur 32%, 23%, and 4.5% of the time, respectively, based on observed product yields as discussed in the text. Pathways D and E are assumed to be negligable because the unsaturated dihydroxyaldehyde products are not seen either by API-MS [32] or the derivatization methods of Yu *et al.* [33]. Pathways B and G are assumed to be of minor importance because we would expect O_2 abstraction from α-hydroxy radicals to dominate over addition, and also there is no evidence for the formation of the predicted $HCOC(CH_3)CHO$ product in the API-MS or derivitization studies. Qualitative product studies [32,33] are consistent with Pathways A, C, H, and I but provide no information concerning their relative importance. In the absence of other information, we assume that each are of equal importance, i.e., occur ~8% of the time. This is not unreasonable in terms of estimated likely branching ratios.

3 See discussion in text and by Aschmann and Atkinson [18]. The species ISO-OX represents 1,2-epoxy-2-methyl-3-butene and 1,2-epoxy-3-methyl-2-butene (see Footnote 35).

4 The $H_2C\cdot OO\cdot$ biradical reacts as in the general alkene mechanism [14,42,43], which in turn is based on data for the O_3 + ethene reaction [24]. The subsequent reactions of formic acid (HCOOH) are ignored.

5 The $CH_2=C(CH_3)CH\cdot OO\cdot$ biradical has no obvious radical fragmentation reaction routes, and 25% is assumed to decompose to propene + CO_2, the other 75% is assumed to be stabilized (see text). The unspecified stabilized product species is represented by the general lumped higher aldehyde species "RCHO". Since RCHO has three carbons and it is being used to represent a 4-carbon product, the unreactive carbon species "-C" is added to maintain carbon balance.

6 Rate constant from Paulson *et al.* [28]. Variation of the radical yield in this reaction within its uncertainty range (10-25%) was found to affect results of model simulations, with the best fits being obtained if the maximum value in the range (i.e., 25%) is assumed. See text for a discussion of the mechanism and footnote 35 for the species represented by ISO-OX.

Table 1 (continued)

7 See discussion in text. RCHO-NO3 is $CH_3C(CH_2ONO_2)=CHCHO$ and IP-MHY is $HOCH_2CH=C(CH_3)CHO$.

8 Rate constant from Atkinson [24]. This reaction is probably not important under atmospheric conditions, but is included for chamber evaluations.

9 This is assumed to react in a manner analogous to NO_3 reaction. The nitro aldehyde product is represented by the nitratoaldehyde product assumed to be formed in the NO_3 reaction to avoid adding new species to the mechanism for this very minor reaction route.

10 Rate parameters recommended by Atkinson [25].

11 Product distribution is based on data and mechanism of Tuazon and Atkinson [38]. 50% of the reaction is assumed to proceed via abstraction from -CHO forming the corresponding acetyl peroxy radical. 42% of the reaction is assumed to involve addition to the 3-position, forming, after an NO to NO_2 conversion, $HOCH_2C(O\cdot)(CH_3)CHO$ which decomposes primarily to HCO and hydroxyacetone. The remainder of the reaction involves initial addition to the 2-position, with ultimate formation of formaldehyde and methylglyoxal.

12 Fragmentation of the primary ozonides in the methacrolein and MVK reactions are based on the HCHO yields of Grosjean *et al.* [44].

13 100% decomposition to form OH radicals is consistent with the measured OH radical formation yield of Aschmann *et al.* [45], if the low yield of this radical as indicated by the HCHO data of Grosjean *et al.* [44] is assumed. Decomposition is assumed to occur via isomerization to $CH_2=C(CH_3)OOH$, which subsequently decomposes to OH and a radical which adds O_2 to form $HCOCOCH_2OO\cdot$, which then converts NO to NO_2 and decomposes to HCHO + $HCOCO\cdot$.

14 The overall quantum yield is treated as an adjustable parameter as discussed in the text.

15 By analogy with the acrolein photolysis mechanism derived by Gardner *et al.* [46], the possible initial reaction processes involve formation of either: (1) $CH_2=C(CH_3)\cdot$ + $HCO\cdot$, (2) $CH_2=C(CH_3)CO\cdot$ + $H\cdot$, (3) $(CH_3)_2C:$ + CO, or (4) $CH_2=CHCH_3$ + CO. For the analogous reactions of acrolein Gardner *et al.* [46] obtained (by complex modeling of their data) roughly equal quantum yields for each of these processes under atmospheric conditions. Assuming that the relative quantum yields are similar in the methacrolein case is probably not inconsistent with the data of Raber and Moortgat [47], except that they observe that the propene forming route is minor. Carbene [i.e., $(CH_3)_2C:$] formation is likely to occur, since otherwise it difficult to rationalize the formation of ethene as a product in the methacrolein photolysis, in ~10% yields [47]. We assume that processes 1-3 are roughly equally important in this mechanism, though this must be considered to be uncertain. The $CH_2=C(CH_3)\cdot$ radical formed in process (1) is assumed to react with O_2 to form HCHO + $CH_3CO\cdot$ (see footnote 45). The $(CH_3)_2C:$ is assumed to react with O_2 to form the excited Criegee biradical $(CH_3)_2C\cdot OO\cdot$, which, based on data for O_3 + alkene reactions [45], is assumed to rearrange to the unsaturated hydroperoxide, decompose to OH radicals and $CH_3COCH_2.$., with the latter reacting with O_2 to form $CH_3CO\cdot$ and HCHO, in a manner analogous to the biradicals discussed in Footnote 13.

16 The NO_3 + methacrolein rate constant has recently been measured to be 4.4×10^{-15} cm^3 $molecule^{-1}$ s^{-1} at 296 ± 2 K [36]. The temperature dependence is estimated. Abstraction from -CHO is assumed to occur with approximately the same rate constant as acetaldehyde, or $k = 2.8x10^{-15}$ cm^3 $molecule^{-1}$ s^{-1} at 298 K [48]. This gives ~50% abstraction from -CHO and ~50% addition to the double bond. Addition is assumed to occur primarily to the 3-position. The $HCOC(CH_3)(O\cdot)CH_2ONO_2$ radical formed is assumed to decompose primarily to HCO + $CH_3C(O)CH_2ONO_2$. The latter is represented by the general alkyl nitrate species RNO3.

17 The product distribution assumed is based on the data and mechanism of Tuazon and Atkinson [37]. The major route is OH addition to 1-position, with the $HOCH_2CH(O\cdot)COCH_3$ radical formed decomposing to $HOCH_2CHO$ + $CH_3CO\cdot$. The methylglyoxal + formaldehyde formation probably occurs after OH addition to the 2-position, though it could also be formed from the alternate decomposition pathway of the $HOCH_2CH(O\cdot)COCH_3$ radical.

18 Interconversion between this biradical and the one formed in the methacrolein system is assumed to occur via a $[CH_3C{=}CH]$ intermediate. The latter reacts as described in Footnote 13.

19 The initial photolysis reactions are based on the data and model of Raber and Moortgat [47]. They found they could simulate products of MVK photolysis under atmospheric conditions by assuming formation of propene + CO occurs ~70% of the time, with the remainder being either formation of $H_2C=CCO\cdot$ + $CH_3\cdot$ or $H_2C=CH\cdot$ + $CH_3CO\cdot$. Although they assumed the latter two fragmentation processes are equally important, we believe that the first is more likely to dominate over the second, and that the data of Raber and Moortgat [47] do not necessarily indicate that the second is occurring to a significant extent.

Table 1 (continued)

20 The MVK + NO_3 rate constant is $<6x10^{-16}$ cm^3 $molecule^{-1}$ s^{-1} at 296 ± 2 K [36], which makes this reaction unimportant under atmospheric conditions.

21 The updated SAPRC mechanism uses absorption cross sections of Rogers [49] and Cantrell *et al.* [50]. See Carter *et al.* [43] and Carter [42].

22 Mechanism based on that for methacrolein. Rate constant and fraction of H-atom abstraction versus OH radical addition for the OH radical reaction is calculated using the estimation method of Kwok and Atkinson [51]. The photodecomposition mechanism was simplified somewhat — only the reactions following the scission of the =C-CHO bond are represented [analogous to process (1) in Footnote (15)]. Because of the faster rates of the competing reactions, photodecomposition of these species is calculated to be relatively unimportant.

23 The rate constant for abstraction from -CHO is assumed to be the same as used for methacrolein. The rate constant for the OH addition to the double bond is estimated using the structure-reactivity estimation methods of Kwok and Atkinson [51]. Both the IP-xxx species are assumed to have the same rate constants.

24 Abstraction from the -CHO group is estimated to occur 25% of the time (Footnote 23). The addition mechanisms are derived using the following assumptions: (1) Addition to the least substituted position dominates. (2) Addition to the least substituted position is 2 times more important than the alternative, based on structure-reactivity estimates [51,52]. (3) Decomposition of alkoxy radicals to form HCO dominates over decomposition to form α-hydroxy radicals, based on results of Tuazon and Atkinson [38] for methacrolein. (4) Decomposition of alkoxy radicals to form the most substituted radical dominates if all else is equal. The products not already in the mechanism are not represented explicitly, but are lumped as follows: $HOCH_2CHOH\text{-}COCH_3$ is represented by MEK, and the two C_4 OH-substituted aldehydes are represented by RCHO + -C.

25 The rate constant is estimated to be in the range $(0.2\text{-}4)x10^{-17}$ cm^3 $molec^{-1}$ s^{-1} by assuming that the k(IP-xxx)/k(2-methyl-2-butene) ratio is approximately the same as the k(acrolein)/k(ethene), k(methacrolein)/k(propene), k(crotonaldehyde)/k(*trans*-2-butene) and k(methacrolein)/k(2-methylpropene) ratios, which are in the range 0.005-0.3 [24]. A rate constant of $1x10^{-17}$ cm^3 $molecule^{-1}$ s^{-1}, the middle of this range, is assumed. The temperature dependence is ignored. Note that the use of this rate constant as an adjustable parameter in the chamber simulations was investigated, but satisfactory results are obtained with using the initially estimated value.

26 Fragmentation of the primary ozonide to form a carbonyl-substituted Criegee biradical is assumed to be similar to those for methacrolein and MVK as indicated by the data of Grosjean *et al.* [44].

27 This is assumed to react in a manner analogous to the mechanism used by Carter [14] for the $CH_3CH\cdot OO\cdot$ See footnote 38.

28 Abstraction from -HCO is assumed to occur with same with the same rate constant as for acetaldehyde, or $\sim 2.5x10^{-17}$ cm^3 $molecule^{-1}$ s^{-1} [24]. The addition rate constant is estimated using a structure-reactivity method analogous to that used by Atkinson [26] and by Kwok and Atkinson [51] for the OH reactions. Based on this, abstraction is estimated to be negligible. The temperature dependence is ignored.

29 Addition is assumed to be to the least substituted bond. When there is a competition among alternative decomposition routes for the β-nitroxy alkoxy radicals formed after O_2 addition and NO to NO_2 conversion, formation of $HCO\cdot$ or $HOCH_2\cdot$ is assumed to dominate over formation of $-CR_2ONO_2$ radicals. The lumped alkyl nitrate species (RNO_3) is used to represent the $HOCH_2(ONO_2)\text{-}COCH_3$ product expected to be formed from NO_3 + $HOCH_2CH{=}C(CH_3)CHO$. The lumped nitrato-aldehyde species (RCHO-NO3) is used to represent $CH_3\text{-}CO\text{-}CH(ONO_2)CHO$ from $HOCH_2C(CH_3){=}CHCHO$.

30 This is assumed to react in a manner analogous to the mechanism used by Carter [14] for the $[H_2C\cdot OO\cdot]^*$ formed in the ethene system.

31 Assumed to react similarly to other disubstituted biradicals such as $[(CH_3)_2C\cdot OO\cdot]^*$, where an excited unsubstituted hydroperoxide is formed, which subsequently decomposes to form OH and other radicals.

32 The mechanism for the atmospheric reactions of furans and their products is unknown, and, in view of its relatively small yield, no attempt is made to derive one in this work. However, it is too reactive a species to ignore completely. The mechanism used in this model is based on the parameterized furan mechanism derived by Carter *et al.* [53] to fit ozone, NO_x, and furan concentration-time profiles in furan - NO_x environmental chamber experiments. No attempt is made to represent chemical processes or product reactions explicitly. To fit the chamber data, any furan mechanism must (1) have a high degree of radical initiation, and (2) have all products formed in significant yields either be unreactive or react extremely rapidly, since once the initially present furan has reacted,

Table 1 (continued)

the system is essentially "dead". The unit quantum yield with the absorption cross-sections of acrolein give the product an extremely short lifetime, as necessary to fit the data. It is assumed that the same is the case for 3-methylfuran. The only difference in this case is that it is assumed that PAN is also formed in the reaction of the product, as a possible fate of the methyl group.

33 The rate constant and OH yield in this reaction have recently been measured by Alvarado *et al.* [54]. The fragmentation process is assumed to involve initial formation of HCO-O-CH=CHCH(.OO.)CH_3, with the biradical decomposing to OH and forming products in a manner analogous to the other methyl-substituted Crigiee biradicals discussed in Footnotes 13 and 15. AC-RCO3. is used to represent HCO-O-CH=CHCO-OO·. The products formed in the unspecified non-radical-forming routes are represented by RCHO, the general lumped aldehyde species in the mechanism.

34 The rate constant of Alvarado *et al.* [54] is used. The mechanism is unknown, but is assumed to proceed in a manner analogous to the OH mechanism, as is the case in the general alkene mechanism [14,42,43], so the same set of products as used for the OH reaction (with NO_2 replacing HO_2, as with the general alkene mechanism) are used.

35 ISO-OX is assumed to consist of 75% 1,2-epoxy-2-methyl-3-butene and 25% 1,2-epoxy-2-methyl-3-butene, based on yield data for both the isoprene + O_3 [17] and $O(^3P)$ [27] reactions. Because the former is the major component, its estimated rate constant, which is assumed to be the same as that for OH + 1-butene [25], is used in the mechanism for the lumped species. In the case of 1,2-epoxy-2-methyl-3-butene, OH addition is assumed to occur primarily in the 4-position, with the O_2 adding to the 3-position to form a β-epoxy alkoxy radical. We speculate that the adjacent peroxy and epoxy centers interact to relieve the ring strain, and that the following decomposition pathway might dominate over bimolecular reactions of this species.

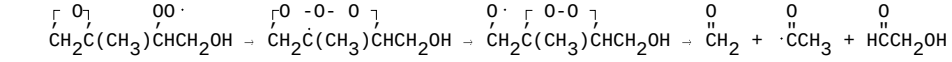

The reactions of the 1,2-epoxy-3-methyl-3 butene would be analogous, though in that case the products would be hydroxyacetone, formaldehyde, and HCO.

36 Atkinson *et al.* [17] measured the rate constant for the O_3 + 1,2-epoxy-3-methyl-3-butene reaction to be 2.5×10^{-18} cm^3 $molec^{-1}$ s^{-1}, which is sufficiently low that this reaction can be neglected. However, the reaction with 1,2-epoxy-2-methyl-3-butene will probably be much more rapid.

37 Assumed to react with the same rate constants and with analogous mechanisms as acetaldehyde.

38 The $CH_3CH{\cdot}OO{\cdot}$ biradical reacts as in the general alkene mechanism [14,42,43], which in turn is based on data for the O_3 + propene reaction [24].

39 Rate parameters recommended by Atkinson [24].

40 Rate constant and mechanism from Niki *et al.* [55].

41 Rate constant of Dagaut *et al.* [56]. Reaction estimated to occur ~95% of the time at the α-OH position using the structure-reactivity methods of Atkinson [52]. The α-OH radical then reacts with O_2 to form methylglyoxal.

42 Assumed to react with same photolysis rate as acetone. The acetone absorption cross section at 330 nm are corrected as discussed elsewhere [42,43].

43 The action spectrum used in the Carter [14] mechanism is still employed, despite the fact that the methylglyoxal absorption cross-sections of Plum *et al.* [57] as used in the that mechanism have been superseded by more recent values [47,48]. The action spectrum derived from the Plum *et al.* [57] (absorption cross-section) x (effective quantum yield) product is believed still to be appropriate because it was based on observed α-dicarbonyl decay rates observed in an environmental chamber. (Errors in the absorption cross-sections are compensated for by opposing errors in the effective quantum yields.)

44 The rate constants for these reactions are from the updated version of the SAPRC mechanism [42,43]

45 This reaction is expected to form CO_2 + $CH_2{=}C(CH_3){\cdot}$. The latter is assumed to react with O_2 to form HCHO + $CH_3CO{\cdot}$ in a manner analogous to the reaction of O_2 with the $CH_2C{=}CH{\cdot}$ radical [58]. Possible reactions of this species are discussed by Tuazon and Atkinson [38], who studied the OH + methacrolein system under conditions where its formation should be important. Although their data ruled out the most likely competing process, there were some inconsistencies with this mechanism, and they conclude that the atmospheric reactions of this radical need further study.

46 Rate parameters from Roberts and Bertman [59].

47 This reaction is expected to from CO_2 + $CH_2{=}CH{\cdot}$, where the latter reacts with O_2 to form HCHO and HCO [58].

48 Assumed to react in a manner analogous to the $CH_2{=}C(CH_3)CO\text{-}OO{\cdot}$ radical.

Table 1 (continued)

49 Assumed to react in a manner analogous to the CH_2=CHCO-OO· radical.

50 Following the treatment of RCHO-NO3 (footnote 7), the mechanism for NA-RCO3. is based on an assumed structure of $CH_3C(CH_2ONO_2)$=CHCO-OO·. Reaction with NO forms CO_2 + $CH_3C(CH_2ONO_2)$=CH·, where the latter is assumed to react with O_2, in a manner analogous to CH_2=CH·, to form CH_3-CO-CH_2ONO_2 + HCO. The nitratoketone product is represented by the lumped alkyl nitrate species RNO3. Since RNO_3 is a 5-carbon species being used to represent a 3-carbon product, -2 -C is added to maintain carbon balance.

[d] The Carter [14] mechanism uses the group of compounds formed from the reactions of peroxy and alkoxy radicals in the presence of NO and the lumped structure group species "-OOH" to represent the reactions of hydroperoxides formed in peroxy + HO_2 reactions.

[e] See Carter [14] for a discussion of the chemical operator approach employed. Note that the species RO2. and RCO3. should be transported and integrated explicitly in the model simulations, but that the steady state approximation can be employed for the other peroxy radical operators and the individual acylperoxy species such as CCO-O2., MA-RCO3., etc.

[f] The RO2. or RCO3. counter species is added to reach reaction forming a peroxy radical to account for their formation rates, and the reactions for them account for their loss rates. Their reactions with the individual peroxy operators (for RO2.) or acylperoxy radical species (for RCO3.) are then used to determine the extent to which these species react with other peroxy radicals. See Carter [14].

Table 2. Acrolein absorption cross sections used to calculate photolysis rates for MVK and methacrolein and the other unsaturated aldehyde products. (Wavelengths in nm, absorption cross sections in 10^{-20} cm^2 $molec^{-1}$, base e.) [a]

λ	σ	λ	σ	λ	σ	λ	σ	λ	σ	λ	σ	λ	σ
280	1.27	295	2.15	310	4.07	325	5.67	340	5.52	355	3.55	370	1.192
281	1.26	296	2.26	311	4.25	326	5.62	341	5.54	356	3.45	371	0.899
282	1.26	297	2.37	312	4.40	327	5.64	342	5.53	357	3.46	372	0.722
283	1.28	298	2.48	313	4.44	328	5.71	343	5.47	358	3.49	373	0.586
284	1.33	299	2.60	314	4.50	329	5.76	344	5.41	359	3.41	374	0.469
285	1.38	300	2.73	315	4.59	330	5.80	345	5.40	360	3.23	375	0.372
286	1.44	301	2.85	316	4.75	331	5.95	346	5.48	361	2.95	376	0.357
287	1.50	302	2.99	317	4.90	332	6.23	347	5.90	362	2.81	377	0.355
288	1.57	303	3.13	318	5.05	333	6.40	348	6.08	363	2.91	378	0.283
289	1.63	304	3.27	319	5.19	334	6.38	349	6.00	364	3.25	379	0.169
290	1.71	305	3.39	320	5.31	335	6.24	350	5.53	365	3.54	380	0.001
291	1.78	306	3.51	321	5.43	336	6.01	351	5.03	366	3.30	381	0.000
292	1.86	307	3.64	322	5.52	337	5.79	352	4.50	367	2.78		
293	1.95	308	3.77	323	5.60	338	5.63	353	4.03	368	2.15		
294	2.05	309	3.92	324	5.67	339	5.56	354	3.75	369	1.59		

[a] These data are available on the Internet by anonymous FTP at cert.ucr.edu, directory /pub/carter/mech.

Table 3. Summary of chambers used for experiments modeled in this work.

Chamber[a]	Volume (ℓ)[b]	Walls	Light Source	Humidity	Refs.[c]
SAPRC ITC	~6400	Heat-sealed, replaceable 2-mil FEP flexible Teflon bag.	Blacklights	~50% RH	A,B
SAPRC ETC	~3000	Same as ITC	Blacklights	dry[d]	B
SAPRC DTC	~5000	Same as ITC. (Dual reaction bags)	Blacklights	dry	B,
SAPRC EC	5774	FEP Teflon-coated aluminum cylinder with quartz end windows	25-KW xenon arc lamp	~50% RH	A,B,C
SAPRC XTC	~5000	Same as ITC	4 6-KW xenon arc lamps	dry	B,D
SAPRC OTC	~40,000	Same as ITC (Dual reaction bags)	Sunlight (run starts ~10 AM)	dry	A,B,D
UNC Outdoor	~150,000	5-mil FEP Teflon film on rigid "A"-frame. Rarely replaced.	Sunlight (run starts at sunrise)	variable	A,E

a Acronyms are as follows: SAPRC = Statewide Air Pollution Research Center at the University of California at Riverside; ITC = Indoor Teflon Chamber; ETC = Ernie's Teflon Chamber; DTC = Dividable Teflon Chamber; EC = Evacuable chamber; XTC = Xenon arc Teflon Chamber; OTC = Outdoor Teflon Chamber; UNC = University of North Carolina.
b For dual chambers (DTC, OTC, UNC), the volume is for each chamber side or bag.
c References: Summary description: (A) Carter and Lurmann [40,41]. Detailed descriptions of chamber and operating procedures: (B) Carter *et al.* [39]; (C) Pitts *et al.* [64]; (D) Carter *et al.* [65]; (E) Jeffries *et al.* [66,67].
d "Dry" refers to the unhumidified output of an air purification system, which is less than 5% RH [39].

Table 4. Initial reactant concentrations in environmental chamber experiments used for mechanism evaluation

Isoprene - NO_x Runs					Isoprene Product - NO_x Runs				
Cham	Run	NO_x	Isoprene	Opt[a]	Cham	Run	NO_x	Methacro	Opt
ITC	ITC511	0.60	1.00	Yes	ITC	ITC513	0.57	2.50	Yes
	ITC811	0.46	0.63	No[b]		ITC819	0.48	1.70	Yes
	ITC812	0.53	0.33	No[b]		ITC823	0.51	3.20	Yes
DTC	DTC053A	0.15	0.30	Yes	ETC	ETC386	0.56	2.20	Yes
	DTC053B	0.24	0.31	Yes	DTC	DTC075A	0.50	4.40	Yes
	DTC056A	0.47	0.71	Yes		DTC075B	0.26	2.40	Yes
	DTC056B	0.47	0.38	Yes	EC	EC651	0.45	1.40	No[c]
EC	EC520	0.49	0.44	Yes		EC652	0.45	0.80	No[c]
	EC522	0.96	0.45	Yes		EC655	0.80	1.50	No[c]
	EC524	1.00	0.87	Yes		EC530	0.43	0.80	Yes
	EC527	0.53	0.42	Yes	XTC	XTC094	0.49	3.90	Yes
	EC669	0.47	0.48	No[c]		XTC102	0.24	1.50	Yes
XTC	XTC093	0.16	0.27	Yes	OTC	OTC317A	0.25	0.50	No[d]
	XTC101	0.53	0.39	Yes	UNC	JN2892R	0.35	2.00	No[d]
OTC	OTC316A	0.42	0.21	No[d]		JN2892B	0.36	0.50	
	OTC316B	0.42	0.43						
	OTC309A	0.21	0.25		Cham	Run	NO_x	MVK	
	OTC309B	0.37	0.25		ITC	ITC512	0.60	2.00	Yes
UNC	JL1680R	0.18	0.80	No[d]		ITC815	0.52	1.80	Yes
	JL1680B	0.19	0.39			ITC816	0.51	0.90	Yes
	JL1780R	0.46	0.20		EC	EC529	0.48	1.00	Yes
	JL1780B	0.46	0.52			EC644	0.49	0.60	No[c]
	JL2381R	0.42	0.29			EC648	0.83	0.90	No[c]
	ST0981R	0.17	0.20			EC649[e]	0.46	1.00	No[c]
	JN2592R	0.36	0.59		XTC	XTC120	0.53	2.00	Yes
	JN2592B	0.36	1.20			XTC121	0.52	0.90	Yes
	JN1793R	0.55	0.94		UNC	JN0892R	0.35	0.50	No[d]
	JN1793B	0.55	0.49			JN0892B	0.35	1.90	

a "Yes" means run used in parameter optimizations as discussed in the text.

b These runs not used in the optimizations because the model fit results were inconsistent with those for the other runs.

c No EC6xx runs were used in the optimizations because of uncertainty in the characteristics of the light source during this period (see Carter *et al.* [39]). In addition, in most cases the model fit results were not consistent with those for most other runs.

d Outdoor runs were not used in the optimization. See text.

e MVK added after two hours in radical tracer-NO_x-air irradiation.

Figure 1. Possible reactions and products in the OH + Isoprene reaction system.

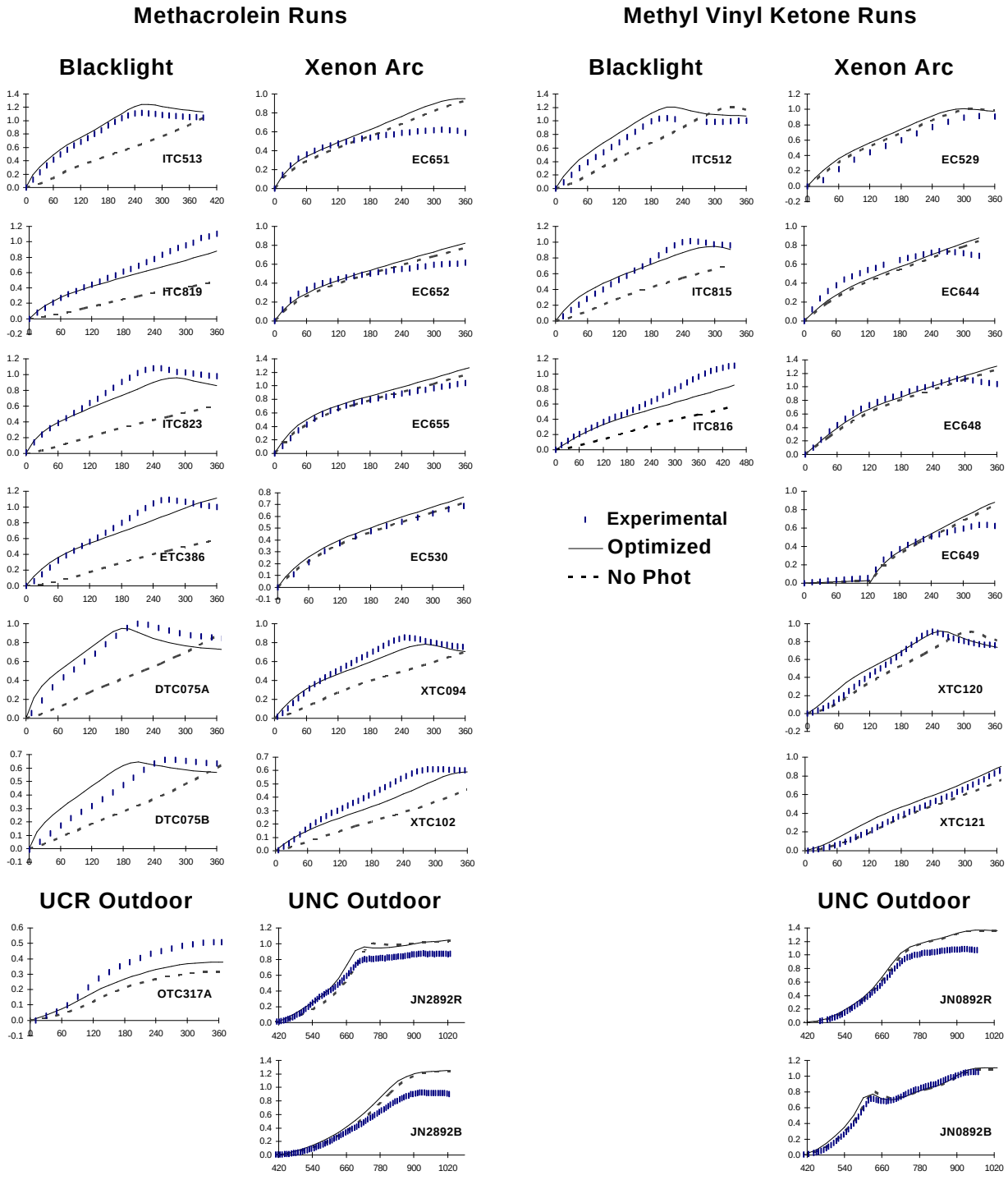

Figure 2. Plots of experimental vs calculated concentration-time profiles for d(O_3-NO) in the methacrolein - NOx and MVK - NOx chamber experiments.

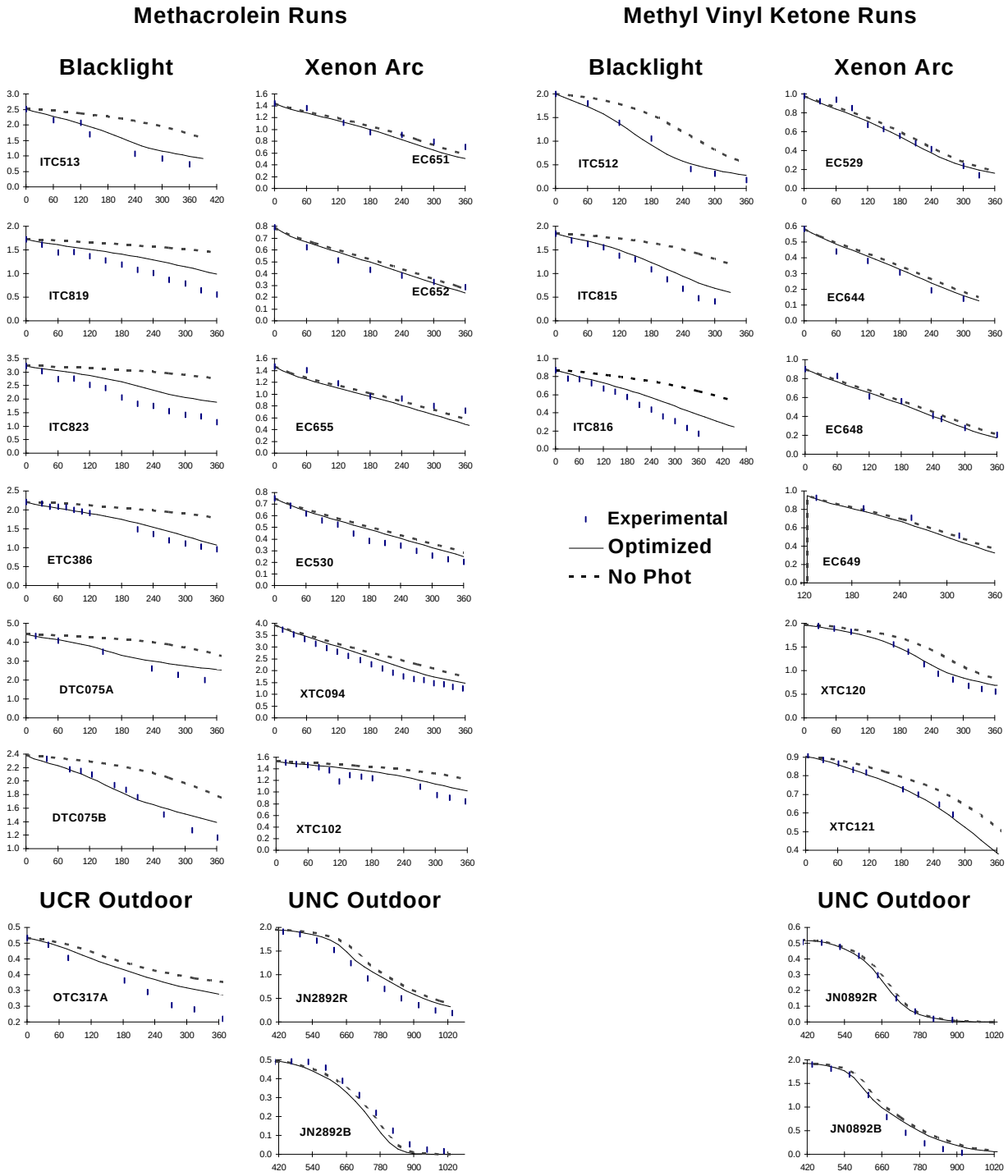

Figure 3. Plots of experimental vs calculated concentration-time profiles for methacrolein in the methacrolein - NOx and for MVK in the MVK - NOx chamber experiments.

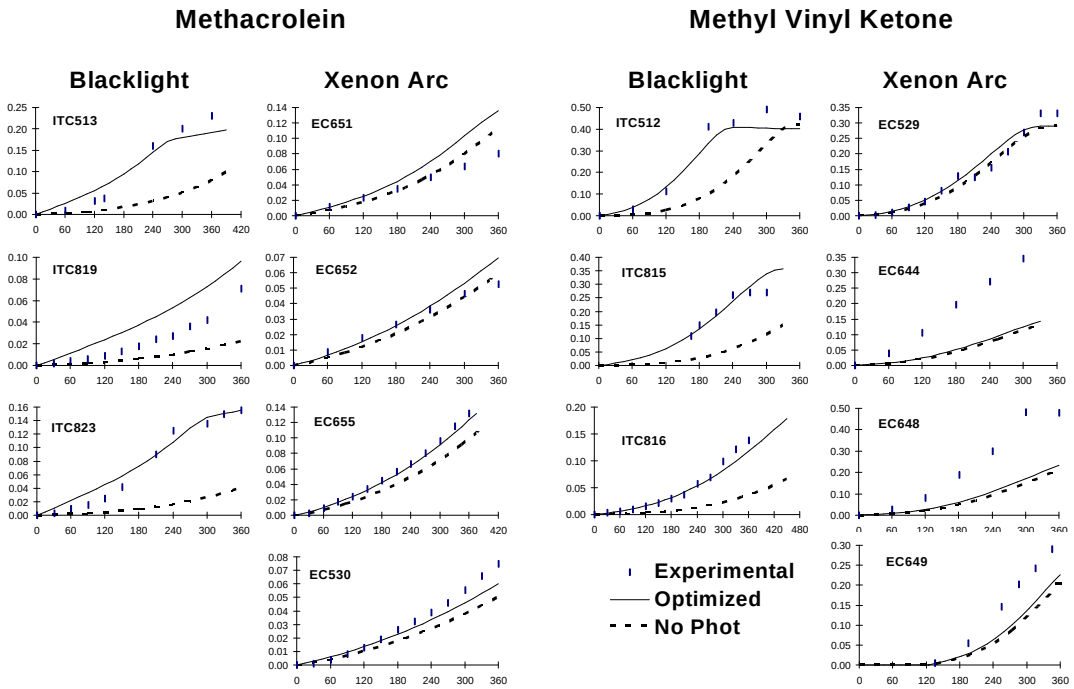

Figure 4. Plots of experimental vs calculated concentration-time profiles for PAN in the methacrolein - NOx and MVK - NOx chamber experiments.

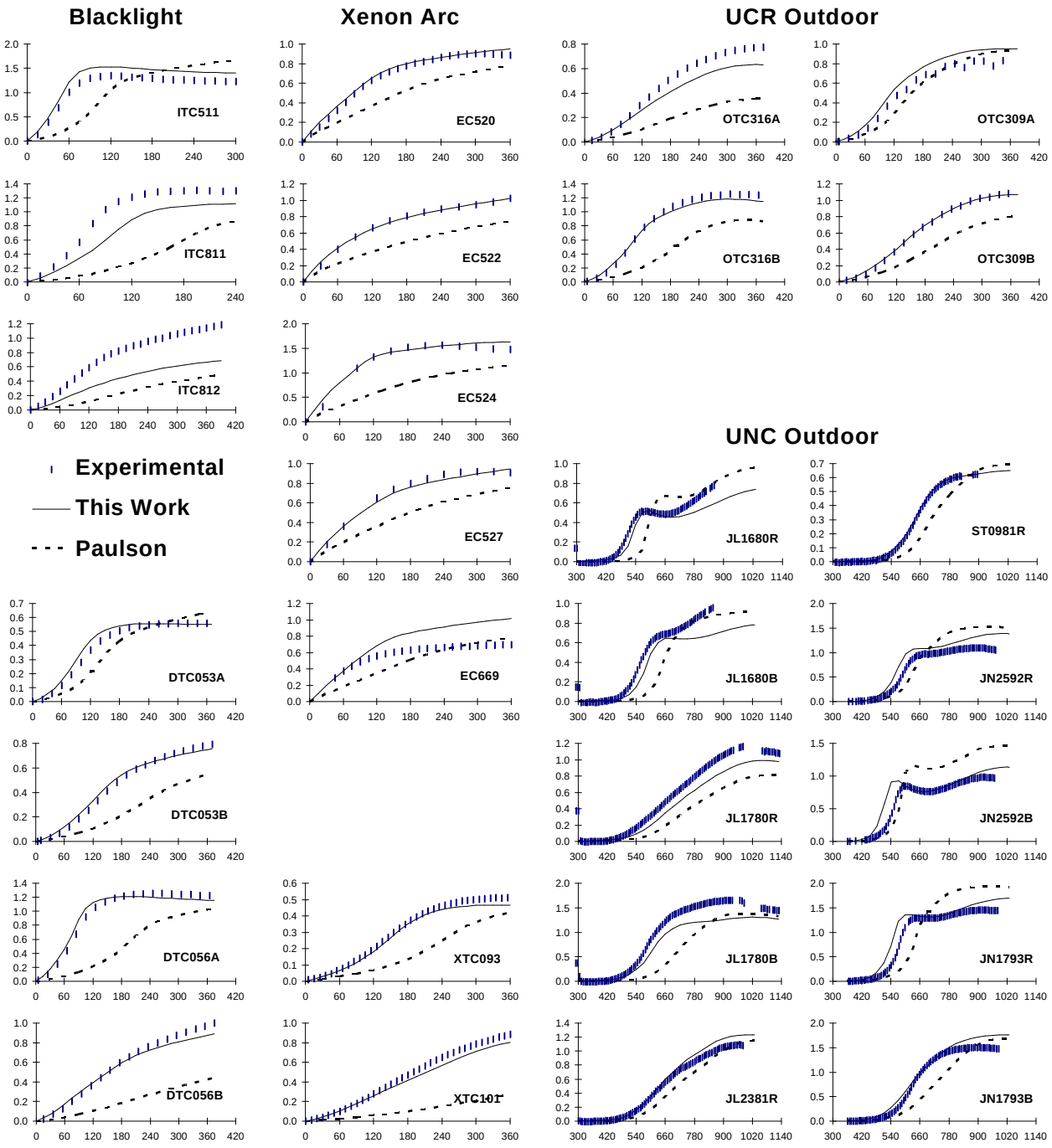

Figure 5. Plots of experimental vs calculated concentration-time profiles for d(O_3-NO) in the isoprene - NO_x chamber experiments.

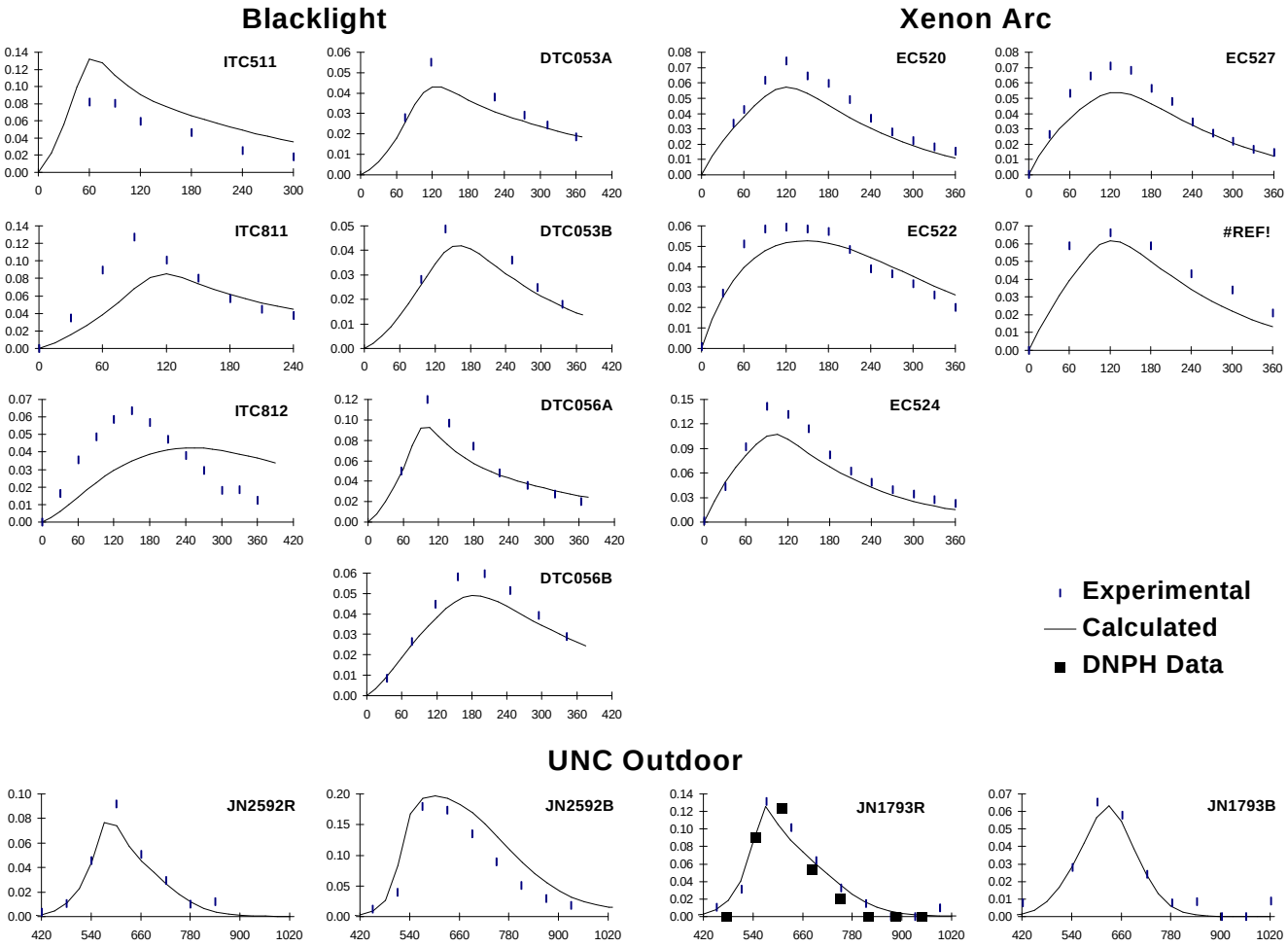

Figure 6. Plots of experimental vs calculated concentration-time profiles for methacrolein in the isoprene - NO_x chamber experiments.

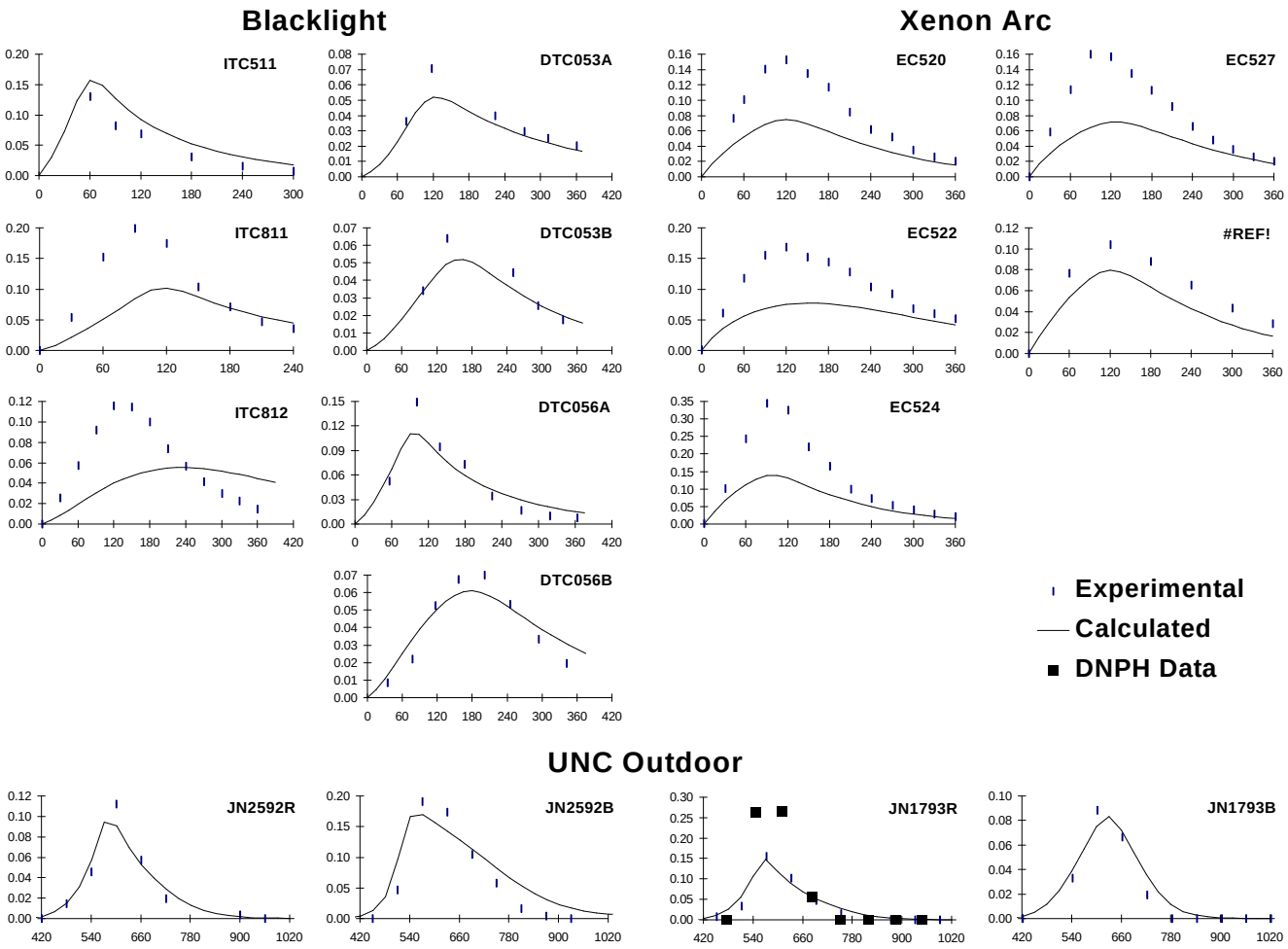

Figure 7. Plots of experimental vs calculated concentration-time profiles for MVK in the isoprene - NO_x chamber experiments.

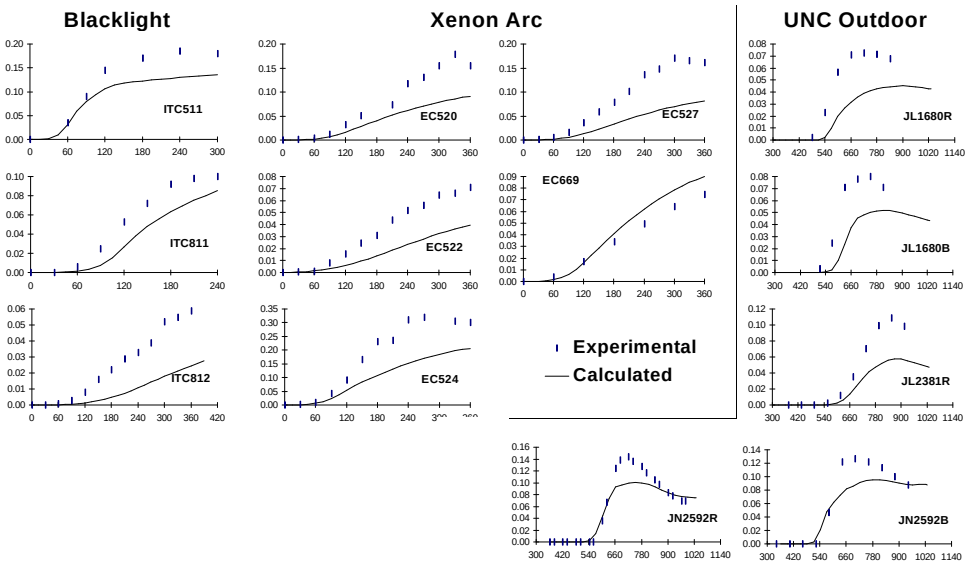

Figure 8. Plots of experimental vs calculated concentration-time profiles for PAN in the isoprene - NO_x chamber experiments.

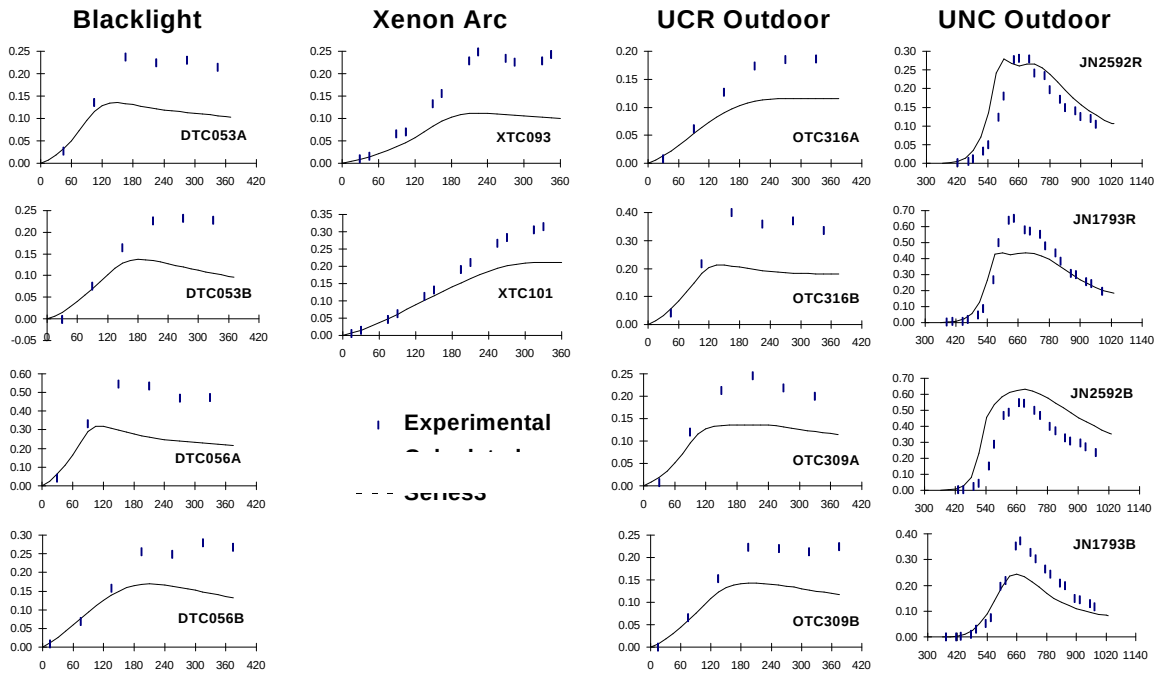

Figure 9. Plots of experimental vs calculated concentration-time profiles for formaldehyde in the isoprene - NO_x chamber experiments.

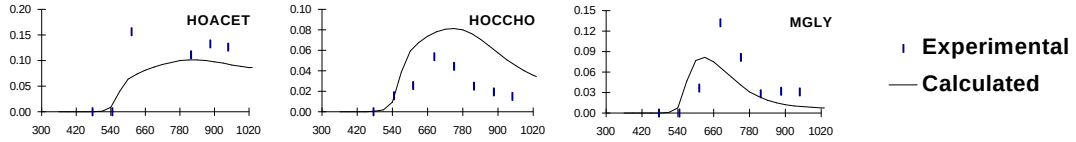

Figure 10. Plots of experimental vs calculated concentration-time profiles for hydroxyacetone, glycolaldehyde, and methyl glyoxal in the UNC isoprene - NO_x chamber run JN1793R.